Assessing soil water content variation in a small mountainous catchment over different time scales and land covers using geographical variables

Florian Mallet, Vincent Marc, Johnny Douvinet, Philippe Rossello, Daniel Joly, Stéphane Ruy

Assessing soil water content variation in a small mountainous catchment over different time scales and land covers using geographical variables

Florian MALLET [(1)*], Vincent MARC [(1)], Johnny DOUVINET [(2)], Philippe ROSSELLO [(3)], Daniel JOLY [(4)], Stéphane RUY [(5)]

[(1)] Avignon Université, UMR 1114 EMMAH, Avignon, France

[(2)] Avignon Université, UMR 7300 CNRS-ESPACE, Avignon, France

[(3)] GeographR, Avignon, France

[(4)] Université Bourgogne Franche-Comté, Laboratoire ThéMA/UMR 6049, CNRS, Besançon, France

[(5)] INRAE, UMR 1114 EMMAH, Avignon, France

** florian.mallet.asterre@gmail.com / + 33 (0)6 59 41 44 88*

Pôle Agrosciences, 301 rue Baruch de Spinoza, BP 21239, 84916 AVIGNON

1 Introduction

Soil water content (SWC) is a key variable in hydrology because it affects soil-atmosphere interactions that control hydrological processes at the catchment scale (Quinn *et al.*, 1993; Bogena *et al.*, 2010). SWC observations are used for data aggregation, hydrological modeling, and upscaling (Romano, 2014) to study processes such as drought (Broedel *et al.*, 2017; Abdelli *et al.*, 2017), flood forecasting (Hapuarachchi *et al.*, 2011), soil-surface exchanges (Tromp-van Meerveld and McDonnell, 2006), rainfall-runoff transformations (Tramblay *et al.*, 2010), and aquifer recharge (Dobriyal *et al.*, 2012). Studying SWC spatio-temporal variability is a challenge because it is determined by numerous factors such as atmospheric forcing, topography, soil properties, and vegetation, which interact differently according to seasons and moisture conditions (Grayson and Western, 1998; Western *et al.*, 2004). Most studies on SWC spatial organization have focused on SWC temporal persistence through the identification of stable patterns (Comegna and Basile, 1994; Mohanty and Skaggs, 2001; De Lannoy *et al.*, 2006; Hu *et al.*, 2010). But in the case of flood generation processes, especially flash flood, the mapping of SWC is required at very short time steps (less than 20 min) to get the event dynamics. For example, event-scale SWC variation maps are needed for the identification of runoff-contributing areas dynamics within catchments. High frequency SWC mapping remains a methodological challenge because areal SWC estimation depends on both the investigation scale and the measurement technique (Robinson *et al.,* 2008) but also on the high heterogeneity of soil in three dimensions.

Several methods have been recently developed to measure SWC at the catchment scale. For example, airborne monitoring has emerged in recent years. These methods are based on remote sensing approaches using passive and active micro-waves as well as radar or multi-spectra waves (Ochsner et.al, 2013) that are characterized by a limited spatio-temporal resolution and accuracy (Brocca *et al,* 2012) even if new generation of SWC estimated from Sentinel-1 are produced at

high resolution in agricultural areas (El Hajj et al., 2017). Indeed, remote sensing provides observations at a resolution coarser than what is required for hillslope monitoring. Moreover, satellite soil moisture is generally representative of surface soil moisture because sensors cannot explore deep through the soil. The development of airborne based sensors (thermal infra-red) makes it possible to monitor soil moisture with higher accuracy and geometric correction has become easier with recent photogrammetry and drone mapping software but sensors and flight missions are expensive and time consuming especially in mountainous environments (Baghdadi, 2005). Space-averaged SWC is also assessed from the non-invasive cosmic ray sensor, which provides time-lapse measurements in a limited area defined by a radius of 300 m around the sensor (Zreda *et al.*, 2008; Bogena *et al.*, 2013; Köhli *et al.*, 2015). But SWC estimation is integrated over a 30 ha area and SWC variation over the measurement area is unknown. Hydrogeophysical techniques such as Ground Penetrating Radar (Huisman *et al.*, 2003; Dubreuil-Boisclair *et al.*, 2011), Electrical Resistivity Tomography (Zhou *et al.*, 2001), multi-temporal resistivity measurements (Brunet *et al.*, 2010) and Electromagnetic Induction (Kashanoski, 1988) have also been used to estimate SWC spatial variability (Michot *et al.*, 2003) on transects, hillslopes, and fields. The pedotransfer function approach has been tested using the relationship between soil electrical resistivity and soil moisture (Brillante et.al, 2014). But SWC retrieval from these techniques is discussed, especially due to their site-dependence (Calamita *et al.*, 2015). At the hillslope scale, recent studies showed that the use of fiber-optic distributed temperature sensing (Selker *et al.*, 2006; Cao *et al.* 2016) could be a valuable approach for 2D observation of soil water dynamics but this innovative method needs a complex calibration procedure according to soil type (porosity, mineralogy, diffusion coefficient) (Krzeminska *et al.* 2012).

In most cases, SWC rate variations across scales have been estimated from a network of local ground-based sensors. In situ SWC plot scale measurements have been greatly improved in the last several decades due to new technologies and devices allowing monitoring in almost all

kind of soils. Invasive methods such as Time Domain Reflectometry (TDR) (Topp *et al.*, 1980), Frequency Domain Reflectometry (FDR) (Jones *et al.*, 2005; Vereecken *et al.*, 2014), and Time Domain Transmissometry (TDT) (Blonquist *et al.*, 2005) make it possible to produce SWC time series along vertical or horizontal profiles (Martini *et al.*, 2017) using soil dielectric permittivity measurements. Nowadays, these probes are usually available at affordable prices and are easy to install in the field. However, significant uncertainties regarding actual values may arise owing to the derivation of SWC from the permittivity measurement or the sensor raw signal *via* calibration equations that depend on temperature and soil texture. Several methods have been proposed to obtain soil moisture maps at higher spatial and temporal resolution from plot scale measurements, primarily based on geostatistical analysis (Western *et al.*, 1999; Brocca *et al.*, 2010), temporal stability analysis (Vachaud *et al.*, 1985; Zhu *et al.*, 2020), the use of empirical orthogonal functions (Jawson and Niemann, 2007), or wavelet coherency analysis (Biswas and Si, 2011). Most of these geostatistical approaches have referred to multiple correlation analysis and variogram models (Ver Hoef, 1993). Geostatistical analyses aim at establishing space-time relationships between SWC and local variables such as porosity or soil electrical conductivity (Kachanosky *et al.*, 1990; Brevik *et al.*, 2006 ; Altdorff *et al.*, 2017), topography as a control of vegetation, soil depth, and by extension, evaporation and evapotranspiration processes (Blyth *et al.*, 2004), or land use (Bardossy, 1998).

Several recent studies using those techniques have investigated the links between land surface characteristics and the spatial distribution of SWC at the catchment scale, as well as the link between topography and SWC/runoff thresholds (Vanderlinden *et al.*, 2012; Penna *et al.*, 2013; Braud *et al.*, 2017). They have highlighted that these controls are very different according to the catchment geographic, climatic and physiographic properties. In a 1.9 km² alpine headwater catchment in the Italian Dolomites, Penna *et al.* (2011) observed that riparian zones reached rapidly saturation and contribute mainly to low runoff ratios. Conversely, high runoff ratios were

associated to subsurface flows on hillslopes occurring during wet period when soils were close to saturation and flowpaths between the hillslope and riparian zone became connected (Sidle *et al.*, 2000; Ocampo *et al.*, 2006; Zuecco *et al.*, 2013; Mallet *et al.*, 2018). This study also showed that during dry period streamflows occurred before SWC reached saturation and conversely during wet period. In a 0.08 km² forested catchment in Pennsylvania (USA), Fan *et al.* (2020) observed that SWC temporal variability was higher on north facing hillslopes compared to south facing hillslopes and that downslope areas were usually wetter than upslope areas. They also observed that SWC became spatially more variable but temporally more stable with depth, which was also observed by Zhu *et al.* (2020) in a subalpine semi-arid catchment in China. The same observation was made between dry warm seasons and wet cold seasons. Slope shape also impact SWC spatial variability, storage and water availability for runoff (Moore *et al.*, 1988; Liu and Luo, 2010; Corrao *et al.*, 2017). Concaved slopes favor water concentrations which lead to higher SWC spatial variability compared to flat areas. Conversely, convex slopes have shallower infiltration depth and lower near surface SWC (Green and Erskine, 2011). Vegetation cover and land use also have a strong impact on SWC spatial and temporal variability since it's highly correlated to topography (Vereecken, 2008). SWC variability among different vegetation types depend on complex variables such as vegetation coverage, root distribution and depth or tree size and spacing (Rodriguez-Iturbe, I., 2000; Ni *et al.*, 2019; Wei *et al.*, 2019; Stevens *et al.*, 2020). Eventually, geostatistical analyses help fill spatial SWC data gaps at the catchment scale but producing high frequency SWC maps at the event time scale in a mountainous catchment remains a methodological challenge (Tromp van Meerveld *et al.*, 2009).

SWC monitoring in sloppy catchments is challenging because they are highly complex. Topography and climatic forcing intensity and variability can make it difficult to access a large area of the catchment. Focusing on the hillslope scale is a way to monitor hydrological processes at smaller scale but some studies warn about the unique behavior of each hillslope which makes

105 their monitoring inappropriate to understand the catchment hydrological behavior (Beven, 2000;
106 Sivapalan, 2003). These studies highlight the heterogeneity of soil hydraulic conductivity, lateral
107 and vertical flow paths, soil depth and layers. To study subsurface flow processes in the Panola
108 Mountains (PMRW, USA), Meerveld *et al.* (2006) developed a complex monitoring on a single
109 hillslope. This kind of monitoring is very effective but difficult to reproduce elsewhere in the
110 catchment because of its cost and extent. In arid badlands, Gallart *et al.* (2013) showed how
111 complex it is to monitor soil water content because of the lack of vegetation and shallow soils.
112 The lack of vegetation associated to sloppy areas induces large erosion rates and mass
113 movements. Intense storms and wind erosion contributes to the development of dense gully
114 network which make it difficult to make long time soil water content monitoring. In the Zin Valley
115 badlands (Israel), Khun *et al.* (2004) studied runoff generation processes on hillslopes without soil
116 water content probes because there is almost no soil layer. Moreover, only extreme rainfall
117 intensities can generate runoff but at the same time high erosion rate.
118
119 In a mountainous, highly erosive environment, previous studies in the Draix-Bléone research
120 observatory have focused on rainfall impacts on runoff and erosion rates (Borges, 1993; Descroix
121 *et al.*, 2003), but also on infiltration processes in heterogeneous marl formations (Garel *et al.*,
122 2012), and on the discrimination of contributing reservoirs to outflow during flood events (Cras,
123 2007). Experiments have highlighted the strong variability of infiltration rates in black marl (from
124 9.E-7 $m.s^{-1}$ to 1E-5 $m.s^{-1}$) and the difficulty of precisely following water fluxes due to the diversity
125 and complexity of the marl structure (Mathys *et al.*, 2006). Moreover, making direct
126 measurements or field observations is not possible during rainfall events due to flash flood
127 hazards. During inter-flood periods, field instrumentation is often damaged due to changes of
128 river morphology or hillslope instability. This situation is common in headwater catchments and
129 explains why soil water content has only been little investigated in such environments. The
130 present study is innovative as it is the first attempt to measure in such environments water

content continuously at the catchment scale and not just on a plot, a hillslope, or a vertical profile. Moreover, measurements are made in different land covers and not only in bare areas.

In this context, the main objective of this study was to explore the short time SWC dynamics in a mountainous highly reactive headwater catchment and its distribution over area from a set of plot scale sensors. A capacitance sensors network has been used to monitor SWC every 15 min at the catchment scale in forest, grassland, and black marl (bare soil) during the summer and autumn periods. The resulting data were used as input in a geostatistical model that links SWC to catchment geomorphological variables by regression and kriging. The specific objectives of the study were to: 1/ analyze how geographical variables influence SWC variations at different time steps, 2/ quantify the relationships between rainfall, SWC, vegetation cover and outflow at the event scale, 3/ examine event scale SWC dynamics among land covers to identify partition between subsurface flow types.

2 Survey area

The study area is the Laval catchment, located within the Experimental Research Hydrological Network Draix-Bléone in the Southern Alps, France (part of the eLTER infrastructure DEIMS.iD: https://deims.org/be7fcb7d-d3c2-486d-a437-4754d18ca1ca). Instruments installed in the catchment have monitored outflow, rainfall and erosion (Fig. 1) since 1983. Outflows are measured at the outlet using a Parshall type gauging station. A rain gauge is installed at the outlet of the catchment while a second one is located on the ridges upstream. A weather station at the outlet of the catchment has provided data on wind speed and direction, solar radiation, relative humidity and air temperature since 2000. Analysis of aerial photographs made it possible to follow bare surfaces evolution since 1948. A first land use map was drawn up by Vallauri in 1997.

Recently, a LidAr survey provided a high spatial resolution DEM (1 m) (Sintegra, 2011). Elevations in this small torrential headwater catchment (0.86 km²) range from 850 m at the outlet to 1200 m. The Laval catchment is known for its high specific discharges during flood events, which may exceed 10 $m^3/s/km^2$ (Mathys *et al.*, 2003). The local climate is sub Mediterranean with continental trend (Joly, 2010) and is defined by high solar radiation (> 2300 hour / year) with mild winters (little snow cover) and very dry summers. Mean annual rainfall is 800 mm (STD = 170 mm; observed period from 1987 to 2015). The local relief and the presence of material that is extremely sensitive to erosion (black marl of Bathonian, Callovian, and lower Oxfordian ages) explain the permanent dense gully network. Rainfall impact varies across seasons with high rainfall intensity during summer storms whereas spring and fall events are characterized by lower intensity and longer duration rainfall. Previous studies have provided detailed information on soil types (Maquaire *et al.*, 2002), soil properties (hydraulic conductivity, porosity, bulk density) (Malet *et al.*, 2005), and black marl sensitivity to runoff (Mathys *et al.*, 2005).

Fig. 1. Survey area - Laval headwater catchment - ORE Draix-Bléone - Alpes-de-haute-Provence - Southern French Alps

3 Material and method

The methodological approach developed in this paper to better understand SWC variation in space and time consists in 3 steps (Fig. 2): 1/ Designing a capacitance sensor network to monitor SWC between 10 and 20 cm depth in various land use and soil types. Once the probes are setup in

the field, they are calibrated using soils samples extracted at each probe location. 2/ Monitoring SWC at a 15 min time step in addition to rainfall and outflow measurements to study the catchment hydrological behavior at the event time scale. 3/ Estimating SWC using a geostatistical model based on geographical variables to represent the probe location situation. 4/ identifying the dominant flow mechanism on hillslopes at the event time scale from the wetting curve maximum slope method (Lozano-Parra et al., 2015).

Fig. 2. Overview of the methodological approach

3.1 In situ measurements

3.1.1 Presentation of capacitance sensors

Selected sub-catchments were equipped for SWC monitoring from May 2016 to November 2016. This investigation was based on FDR probes (10HS by *Decagon Devices* ®). Less expensive than TDR and relatively easy to set in the soil, the 10HS probe makes it possible to measure SWC continuously on large scale through a network of autonomous sensors. The soil and the probe electrodes are used as a capacitor whose capacity varies according to the soil dielectric permittivity which is related to the presence of water (Qu et al., 2013). The sensor uses a 70 MHz frequency that minimizes salinity and textural effects, and the 10 cm long probe has an influence volume of about 1.3 liter. Fourteen capacitance probes were set up in different soil types in the survey area: 4 in the black marl, 4 in grassland, and 6 in forest (Table 1). The monitoring was carried out using a 15 min time step. The 10HS probes were vertically positioned to give an average SWC between -10 cm (bottom of electrode) and -20 cm (top of electrode) depth. At the plot scale, SWC was also measured vertically using PR2 probes (*Delta-T Devices* ®). These sensors were carried on to different points and measurements were done into a plastic tube. SWC were

obtained at four depths (10 cm, 20 cm, 30 cm and 40 cm) by measuring the dielectric constant of the soil using capacitance/time domain technology. Vertical monitoring from May to June 2016 showed that most SWC variations occurred between 10 cm and 20 cm in grassland and forest in the study area. It is important to note that some astonishing behavior could be monitored due to improper set up. Indeed, FDR probes present a high sensitivity to soil contact and can be strongly impacted in case of air gaps between the soil matrix and the sensor. Air gaps are due to black marl structure complexity and instability near surface, to stones and tunnels created by animals especially in grassland, and mainly to roots and stones in forest, but also to freeze/thaw process (Mallet, 2018).

Table 1. Soil type and properties at the plot scale

Plot	Land Cover	Classification (INTL)	Porosity	Bulk density (kg/m^3)	Slope	Orientation
B1	Black marl	Clay loam	0.302	1.86	30	SE
B2	Black marl	Clay loam	0.356	1.73	10	S
B3	Black marl	Clay loam	0.409	1.55	25	NE
B4	Black marl	Clay loam	0.414	1.54	30	NE
F1	Forest	Silty loam	0.469	1.40	5	S
F2	Forest	Silty loam	0.434	1.49	15	W
F3	Forest	Silty loam	0.452	1.45	15	N
F4	Forest	Silty loam	0.502	1.32	15	N
F5	Forest	Silty loam	0.447	1.46	15	N
F6	Forest	Silty loam	0.494	1.36	20	NW
G1	Grassland	Silty clay loam	0.498	1.33	15	S
G2	Grassland	Silty clay loam	0.457	1.40	20	SW
G3	Grassland	Silty clay loam	0.466	1.41	20	SW
G4	Grassland	Silty clay loam	0.457	1.41	10	SE

3.1.2 Calibration of 10HS capacitance sensors

SWC values were obtained from soil electrical permittivity, which was computed from the raw 10HS probe signal. SWC data obtained from 10HS probe using the third-order polynomial calibration function provided by the manufacturer (Decagon Devices, 2016) were compared to water content values extracted from in situ soil samples collected from depths of -10 cm to -20 cm. Soil samples were collected from each plot scale using 10 cm long cores (from -10 cm to -20 cm depth) under different hydric conditions. Results showed that SWC monitored in forest fitted the manufacturer theoretical law. A different calibration function was developed from soils sampled in grassland and black marl (Mallet *et al*., 2018). Sensor accuracy was found to be +/- 3% in forest and +/- 4% in grassland and black marl, which is a reasonable estimate of mean SWC patterns at the watershed scale.

3.1.3 Network optimization

Studying spatial variability of water content in the upper soil layer is a complex task as it strongly depends on the scale of analysis. Using a sensor network continuously measuring SWC makes it possible to get spatial data at small scales such as plots, transects, hillslopes and small catchments. Regarding the Laval catchment size, the survey budget, manpower, and the distance from the lab to the experimental field, a network of few sensors was setup to provide data at the plot scale (Blume *et al.*, 2009). To optimize the spatial distribution of the network, homogeneous soil-landscape patterns with potentially specific hydrologic behaviors were delineated (Dehotin and Braud, 2008). Such landform-units were defined according to hydrological criteria (stream network and sub-catchment classification), land cover, soil type, and topography (slope, hillslope orientation). In this study, a four-step method has been applied (Fig. 3) as follows:

263

264 **1**/ Sub-catchments were delineated using the Strahler stream network classification
265 (Strahler, 1952; Le Barbu, 2006). Only sub-catchments of order 3, 4 and 5 whose main talweg is
266 connected to the main network were selected for this stage. They represent a minimum surface
267 of 1 ha which exceeds the surface of an elementary gully whose hydrological behavior is already
268 known (Mathys, 2006).

269

270 **2/** Theoretical surface flow concentration areas were then mapped using the RuiCells cellular
271 automaton (Langlois and Delahaye, 2002) which establishes a link between topographic variables,
272 the catchment morphology (size and form), and hydraulic variables. Using a 10 m DEM (1 m DEM
273 could not be used because of the model computational capacities), a spatially homogeneous
274 rainfall, and considering a zero infiltration capacity of the soil, Ruicells produces a surface flow
275 concentration map. Surface flow concentration is computed at each sub-catchment outlet by the
276 Concentration Index (CI) which takes into account the density of the stream network upstream of
277 each sub-catchment outlet (Douvinet *et.al*, 2015). The produced map makes it possible to better
278 understand the catchment potential hydrological response from the sub-catchment to the final
279 outlet (Douvinet, 2008). For instance, very marked surface water flow concentrations (CI > 10) can
280 be observed at the outlets of several sub-basins of orders 3, 4 and 5 and at several confluences (in
281 the main network) while some sub-catchments show very low IC index. This step highlights the
282 heterogeneity of the catchment potential hydrological response and helps to identify potential
283 SWC measurements plots.

284

285 **3**/ The percentage of bare and vegetated surfaces (forest, grassland) was then calculated on
286 the sub-catchments and compared with the potential surface flow concentration areas identified
287 in step 2. Sub-catchments marked with CI> 10 have various land covers: the proportion of
288 vegetated areas varies from 11% to 82%, while bare soils are between 17% and 88%. It is

therefore interesting to target the investigation on sub-catchments with various CI and land cover. Eventually, four sub-catchments with various size, morphology, land cover, soil types and network ordination were selected for the investigation.

4/ Soil type map (Maquaire et.al, 2002) was then combined with land cover map which made it possible to identify the most represented land covers within the Laval basin. In order to concentrate the analysis on the most represented soil-vegetation units, only the first six classes obtained were retained which represent 72.9% of the Laval total surface.

5/ SWC probes were then setup in the six classes identified in step 4 within the selected sub-catchments in step 3. Final probe location depended on slope, hillslope orientation, and accessibility.

Fig. 3. A four-step method to obtain an optimal capacitance sensors network in the study area

Comparison of SWC values requires homogenous spatial distribution of rainfall over the catchment at the event scale. For this purpose, rainfall spatial variability was studied at the event scale with the addition of 3 rain gauges (*Rainwise*®) set up inside the catchment away from vegetation cover (Fig. 2). Their location was based on elevation, distance to the outlet, and accessibility (Table 2). Fourteen rainfall events were studied in 2016. For each event, each rain gauge data were compared to data measured at the catchment outlet (*Précis Mécanique* ®).

Table 2. Laval rain gauges

Rain Gauge	Setup	Elevation (m)	Distance from outlet (m)
P0	1984	851	0

P1	2015	900	690
P4	2015	890	380
P6	2015	915	878

3.2 Geostatistical modeling framework

3.2.1 Presentation of LISDQS

The LISDQS (Interpolation of Quantitative and Spatial Data) geostatistical model (developed by Joly and Vuidel in 2008 and presented in Joly *et al.*, 2008) was used to estimate SWC at the plot scale considering local geographical variables (Arnaud and Emery, 2000). LISDQS runs a global analysis that computes all measurement plots to produce a single geostatistical model fitting for all plots at each time step. Spatial interpolation of soil moisture measurements is performed by the combination of linear regressions (LR) (Joly *et al.*, 2011) followed by kriging of the residuals using the method « regression-kriging » (RK) described by Hengl et al. (2007). LR is used to fit the explained variation with spatial predictors. The subsequent kriging process used to fit the residuals, i.e. unexplained variation, is ordinary kriging fitted by a single variogram (Spherical model) (Matheron, 1970; Gratton, 2002).

3.2.2 A three-step analysis method

The LISDQS model combines kriging and regression in 3 steps: 1/ Linear Regression between all SWC plot and local variables (topography, vegetation, soil) reveals the variables that best explain the SWC space-time variations (highest R^2 for $P_{value} < 0.05$). These best explanatory variables are then associated 2 by 2, 3 by 3, 4 by 4, etc... (from the best to the worst) in stepwise

multiple regressions (Hocking, 1976). The best combination (with the highest R^2) is applied to all plots to obtain estimated values that are compared to measured values. 2/ Kriging shows the spatial structure of SWC distribution of residuals obtained in the first step. Kriging uses the semi-variogram properties and also computes residuals. 3/ Third step is Residual Kriging. At the end of the first step (LR) and the third step (RK), the estimated soil moisture values are validated by a "leave-one-out" cross-validation (Plutowsky *et al.*, 1994), the process of which is as follows: as many iterations are repeated as there are observations *i*. At each iteration, observation *i* is removed from the sample and the model runs with the new sample. Then using this new model, the predicted value of the withdrawn observation *i* is calculated. A series of predicted values is then obtained which can be compared with the observed values by calculating the residuals of the model. The residuals obtained at the end of phase 1 are estimated by kriging, those obtained at the end of phase 3 are used to estimate root-mean-square error (RMSE). This three-step method makes it possible to improve the spatial interpolation of SWC data by taking into account environmental heterogeneity.

3.2.3 Parameterization

The LISDQS geostatistical model automatically performs a sensitivity analysis for each time step. Linear regressions were computed between SWC measured at the plot scale and the mean value of local variables on a 9 m² area around the plot. This averaging method accounts for the environmental heterogeneity around the SWC probe and not only the value of a 1 m² plot. The linear regressions make it possible to identify the best variables among as many variables as needed to be tested.

SWC was driven by a set of local variables that are used in the geostatistical model. These variables drive different processes that affect SWC variations according to seasons and soil

367 moisture status. A high-resolution Digital Elevation Model (DEM) (LiDAR, 1m, Panissod *et al.*,
368 2010) was used to derive 4 topographic variables: curvature index (slope convexity or concavity),
369 soil depth, hillslope orientation defined by sinus (West-Est orientation) and cosinus (North-South
370 orientation). The Normalized Vegetation Index (NDVI) was computed from a SPOT 6/7 image[1] to
371 take into account the land cover influence. It is the most common vegetation index for identifying
372 areas with an elevated chlorophyll activity which are related to vegetation. It computes the
373 difference between red and near-infrared wavelengths and is normalized by the addition of both
374 which reduces the ground lightness. NDVI was calculated from the only SPOT image that covered
375 the survey area during the study period.
376
377 Cross correlation analysis showed that the NDVI was positively correlated to solar theoretical
378 radiation which gives for each DEM pixel the solar radiation in W/m² at different time scales. The
379 latter was weakly positively correlated to hillslope orientation (R = 0.55), whereas slope was
380 negatively correlated to NDVI (R = - 0.415) (Table 3). In the study area, gentle slopes are mostly
381 associated with vegetation, which are also among the sunniest areas, while steep slopes are
382 mostly associated with gullies and bare areas. Soil depth was positively correlated to NDVI (R =
383 0.58) because soils develop with vegetation growth, whereas bare areas are prone to erosion.
384 NDVI is related to interception and evapotranspiration, slope affects subsurface flows (horizontal
385 or vertical), and solar radiation is associated to evapotranspiration whereas soil water storage
386 mostly depends on soil depth. The solar radiation curve followed the same dynamic as NDVI and
387 had an increasing positive correlation with SWC from July to mid-October. Soil depth had a stable
388 positive correlation with SWC over the study period.
389
390 **Table 3. Correlation (R) between explanatory variables used for the geostatistical modeling.**

[1] *Contains informations © 2014, Distribution Airbus Defense & GEOSUD, France, all rights reserved.*

	Sinus	Cosinus	NDVI	Curvature	Soil depth
Sinus	1	0.081	-0.538	-0.034	0.308
Cosinus		1	0.109	-0.04	0.631
NDVI			1	-0.286	0.598
Curvature				1	0.293
Soil depth					1

3.3 Identifying the dominant flow mechanism

Previous studies showed that surface runoff was the main hydrological processes during flood event in the Laval catchment. However, subsurface flow processes also play a key role on the catchment hydrological behavior. During rainfall, preferential flows contribute to fast wetting of shallow soil horizons and to outflows by rapid exchange from soil to streams. On the other hand matrix flows can be observed anytime and in every monitored land covers and affect soil moisture status and water availability for plants. During a rainfall event those two processes can occur simultaneously. To identify the dominant process, the method of the wetting curve maximum slope (*Smax*) as proposed by Lozano-Parra *et al.* (2015) was used. This analysis aims at identifying which process is dominant, but not to quantify its contribution to discharge.

$$S_{max} = max\left(\frac{\theta_{t+\Delta t} - \theta_t}{\Delta t}\right) * 10^4$$

This parameter represents the maximum soil water content increase measured at the event time scale by each probe between two measurements. θ_t is the SWC value at the time t, and Δt is the 15 min interval between two measurements. *Smax* was used as an indicator for the degree of slow or fast flows. On this base, it was assumed that low *Smax* value was representative of matrix

flow while high *Smax* was associated to preferential flow (Fig. 4). Intermediate slopes were associated to a mix of both processes.

Fig. 4. Examples of different soil moisture increases monitored during three different flood events.

4 Results

The results are divided in four sections that address the questions proposed in this paper. First, rainfall variability was studied to ensure that SWC data obtained at different locations could be compared and that the geostatistical analysis could be conducted. Then relationship between SWC and discharge was analysed to take into account the catchment near-surface hydric status impact on the catchment hydrological response. Measured and estimated SWC data obtained at daily, hourly and 15 min time scales were then compared to see how geographical variables could be used to determine SWC at the catchment scale under various land use and hydric conditions. Eventually, SWC variations at 15 min time step were analysed and compared to rainfall properties to enhance SWC space-time variation and impact on subsurface flow types.

4.1 Low rainfall spatial variability at the event scale

The event scale analysis showed low variability between the 3 rain gauges inside the catchment (differences ranged from 0.3% to 3.4%) (Fig. 5). On the other hand, differences (from 0.4% to 21.5% of the cumulative rainfall event) occurred between P0 (located at the final outlet) and the other rain gauges, with higher cumulative values measured at P0 at the event scale (mean difference of 6.3%). The largest differences occurred during April 22 and June 16 events with cumulative rainfall lower than 31.2 mm (measured at P0). These differences come from the smaller diameter of P1, P4 and P6 compared to P0. The low spatial variations at the event time

443 scale showed that rainfall was relatively homogenous over the catchment, which made it possible
444 to conduct the geostatistical analysis at the event scale.
445
446 **Fig. 5. Cumulated rainfall monitored by 4 rain gauges for 14 rainfall events in 2016. The number over the bar chart is**
447 **the difference between the highest and the lowest rainfall values recorded by the rain gauges at the event time scale.**
448 **No rainfall data available on February 7 and March 5 at P4 gauge.**
449
450 **4.2 Relationship between SWC and discharge**
451
452 Daily SWC variations provided an overview of the catchment wetting/drying dynamics
453 over the study period (Fig. 6). Significant differences between measured SWC were observed
454 among the three main land cover types.
455
456 SWC dynamics were similar in vegetated areas although a higher dispersion of SWC values
457 was observed between forest plots (mean SWC difference of 3.9% between F1 and F4) as
458 compared to grassland (mean SWC difference of 0.3% between G2 and G4) because forest
459 sensors are setup on silty loams which have a higher water capacity than the other soils. F1 and
460 F2 sensors globally monitored less variations than the other sensors located in forest. Soil
461 evaporation which has been taken into account by the sensor placed at 10 cm has a strong
462 dynamic especially during wetting period. While during dry period plants extract water in deeper
463 layers and the sensor monitor less variations. It could also be explained by improper installation
464 since F1 and F2 are installed in soils with a lot of roots and stones. The highest daily SWC was
465 measured in forest (SWC = 41.8%) but the SWC variation (SWC max - SWC min) was lower than in
466 the other land covers (SWC values ranging from 20.8% to 41.8% in forest, from 11.2% to 34.8% in
467 grassland, and from 1.8% to 30% in black marl areas).
468

SWC dynamics was quite different among black marl plots (mean SWC difference of 8.7% between B1 and B2). SWC showed high amplitude (min = 2.5%; max = 30%) but daily SWC variations was smoother than what was observed in rooted soils. Only the B2 probe, located between bare soils and rooted soils, had a similar trend to that of vegetation probes with a short reaction to rainfall. The high variability of SWC across space and time in black marl showed that black marl had the capacity to store and release water during the entire study period which can be explained by the complexity of subsurface exchanges in this medium. This can be explained in particular by the spatial variability of infiltration between the different types of regoliths. Saturation hydraulic conductivities measured on hillslope summit were low which favored surface runoff. Saturation hydraulic conductivities measured on footslopes where weathered marl accumulated were higher and more propitious to infiltration (Mathys and Estèves, 2005).

During the study period, each rainfall events resulting in a flood event (Qmax > 500 l/s) provoked variations on all SWC probes measurements (Fig. 6) as expected since rainfall was found to be quite homogeneous over the catchment. Conversely, some rainfall events did not led to outflow variations despite variations recorded on SWC probes. Between May and the end of November, only 7 rainfall events on a total of 16 with cumulative amount over 30 mm gave rise to floods with discharges over 500 l/s (except for the September 12 event with 18 mm rainfall amount). This rainfall threshold is consistent with past observations (Mathys, 2006).

Fig. 6. SWC time-series data presentation. Daily mean SWC is monitored at 14 plots. River flows are measured at the Laval outlet by a Parshall flume. Rainfall was measured from May 11 until November 29 2016 at the Laval final outlet. Dashed lines indicate flood events (Discharge > 500 l/s).

These catchment outflow variations partly depend on the relative soil dryness/wetness which controls the occurrence of overland flows on the hillslopes. Based on the total volume flowed over the event, this relationship is evidenced by the positive trend observed between the

initial water content and the runoff coefficient, except for the most exceptional flood events where direct surface runoff occur over the main part of the event (Fig. 7, red dot). Peak discharges are usually higher in autumn when the catchment is wet than in summer due to higher cumulative rainfall in autumn compare to summer rainfalls. However, no correlation was observed between the initial soil moisture and the maximum flow rate reached at the outlet. This result illustrates the variability of runoff conditions on the slopes at the peak discharge which change highly according to the events (dominant contribution of hortonian flow or subsurface flow).

Fig. 7. Relationships between runoff coefficient and antecedent soil moisture at the event time scale. The runoff coefficient is the ratio (%) between the amount of water flow and the amount of water precipitated at the event time scale. Antecedent soil moisture is an average value computed from the values of each capacitance probe before rainfall.

4.3 Estimated SWC at daily and hourly time scales

4.3.1 Observed SWC VS estimated SWC

To validate the geostatistical modeling, the model was run using SWC data from 11 sensors instead of 14. Then the 3 remaining sensors (one in forest, one in grassland and one in black marl) were used to validate the model at the daily and hourly time scales which gave similar results (Fig 8). SWC were well estimated in all land uses throughout the study period. The mean error (+/- 2.3%) was lower than the in situ measurement error (from +/3% to +/- 4%). In spring, especially in May, SWC values were underestimated in all land uses. In summer, estimated SWC values fitted quite well with observations until August and early September rainfalls where estimated SWC values were overestimated in grassland and underestimated in forest and black

523 marl. Estimated SWC values appeared to be overestimated in grassland throughout fall especially
524 from mid September until mid October. Conversely, estimated SWC values fitted with
525 observations in forest and black marls despite underestimations in forest the days after long
526 autumn rainfalls.
527
528 **Fig. 8. Model validation at daily and hourly time scales.**
529
530 Measured and estimated SWC values were compared using the linear least squares
531 regression method. Variation of the determination coefficient (R^2) gives an overview of the
532 statistical analysis and how geomorphological variables can be used to estimate SWC variations
533 over different time scales (Fig. 9). However, R^2 values must be interpreted with care since there
534 are only 14 data points in the regressions. First of all, correlations between measured and
535 estimated SWC were better at the hourly time scale in May and June and from the October 14
536 flood event until the end of November (catchment wetting period) while relationships were
537 better at the daily time scale during summer (catchment drying period). SWC variations often
538 appeared at the same time with higher amplitude at the hourly time scale and a smoother
539 dynamics with the daily data. In most cases, higher correlations were observed during no rainy
540 periods, namely during soil drying by drainage or evaporation losses. However, sharp decreases of
541 R^2 were observed at both time scales during flood events. The loss of correlation with the
542 catchment morphological features at that times shows that SWC variations were mostly
543 controlled by rainfall intensity.
544
545
546 **Fig. 9. Relation between measured and estimated SWC (R^2) at daily and hourly time scales. R^2 were computed at both**
547 **daily and hourly time scales by plotting the 14 measured SWC with the 14 estimated SWC to get one R^2 value every**
548 **time step. The relationships are significant over the "Student" red dot line.**
549

Time series plots show that SWC were generally correctly simulated in all land covers (Fig. 10). Nevertheless, a few probes showed singular behaviors. For instance, B1 probe (black marl) was poorly simulated (R^2 <0.4) compared to B3 and B4 probes. Also, B1 probe measured very low SWC values from summer until the end of September while B3 and B4 were highly reactive to the first autumn rainfall event (September 12). It could be explained by improper setup and air gaps between the marl and the probe electrodes since B1 is installed between marls layers. This installation was hard but it was important to monitor that kind of zone since it is highly represented at the catchment scale. Measurements obtained at this location need to be interpreted with caution. In grassland, G1 probe showed a very low R^2 (< 0.2) with lower values and larger variation of the simulated SWC compared to observations. Conversely, F1 probe set up in forest measured higher SWC values and much lower variations than the estimated SWC. These shortcomings were assumed to be the result of improper set up.

Fig. 10. Some examples of relationships between measured and estimated SWC (R^2) at some plots in various monitored land covers at the hourly time scale.

4.3.2 Weight of local geographical variables in the geostatistical model

At both daily and hourly time scales, the weighted model gives information about wetting/drying processes using mainly 3 variables: soil depth, curvature index and NDVI. During wetting periods, the model estimated SWC by combining mainly curvature index and NDVI (Fig. 11), except during high flows where rainfall intensity had a major impact on SWC variations. During drying periods, SWC was primarily estimated by combining soil depth and NDVI. NDVI weight never exceeds 20% but is constantly used over the study period as it is related to interception, evaporation and evapotranspiration processes. Curvature index controls drainage

processes and has a strong weight in the model during rainfall and from mid October until mid July. Soil depth has a strong weight from mid July until mid October as it is linked to recharge processes by controlling soil water storage capacity. In early fall (mid September until mi October), the weighted model varied using mainly soil depth, curvature index and cosinus (which is related to soil depth (R = 0.631)). No flood event appeared during this period but grouped rainfall events leaded to successive wetting/drainage processes at short time steps.

Fig. 11. Representation of the primary weighting of local variables in the weighted model at both daily and hourly time scales.

4.4 Estimated SWC at event time scale (15 min)

4.4.1 Observed SWC VS estimated SWC

The overall relationship between measured and estimated SWC was computed from all 14 capacitance probes for each of the 7 flood events that appeared from may until November 2016 (Fig. 12). The relationship is statistically significant over a threshold of $R^2 = 0.53$ ($P_{value} = 0.05$). At a 15 min time step, correlations between measured and estimated SWC (R^2) had the tendency to decrease when rainfall intensity increased and in return to increase when rainfall stopped or intensity was very low (< 2 mm/h at a 15 min time step). This increase of R^2 during drainage is consistent with observations made at the daily and hourly time steps. R^2 decreases were larger at the beginning of rainfall events. For instance, a rainfall intensity of 8 mm/h occurring at the beginning of the storm induced a higher R^2 decrease than a rainfall intensity of 40 mm/h that happened almost 2 hours after the rainfall began (Fig. 12, October 14 event). The same

observations could be made during a long autumn rainfall (840 min) where a maximum rainfall intensity of 8 mm/h (at a 15 min time step) during the first part of the event caused a higher R^2 decrease (from 0.8 to 0.6) than a maximum rainfall intensity of 10 mm/h (at a 15 min time step) that occurred later (Fig. 12, November 21/22 event). Also, a delay was observed between rainfall and R^2 variation induced by infiltration time and the different SWC rising times (for each probe, time between the beginning of rainfall and the change of the slope in the SWC rising). This delay was negatively related to rainfall intensity. SWC were better estimated during November storm flows caused by long rainfall events with low intensity when the catchment was wet (high mean SWC and low SWC variations). During summer, flood events caused by shorter and more intense rainfall when the catchment was dry (high SWC variations) resulted in poorer correlations.

Fig. 12. Overall relationships between measured and estimated SWC (R^2) at the event time scale.

Time series plot shows that SWC dynamics were well estimated in most situations (Fig. 13). Observed values were underestimated or overestimated according to the plot with a maximum deviation of about 5% water content. Nevertheless, singular behaviors were observed at few plots such as the absence of SWC reactions to rainfall (e.g. F1 and F2 probes) despite measurements recorded by the closest rain gauges under vegetation cover (10 m from F1 and 70 m from F2). This could be explained by soil hydrophobia due to the absence of rainfall event since 8 days. Moreover, no rainfall with amount over 6.8 mm happened since 16 days. Hydrophobia had already been observed in July 2015 during soil infiltration experiments.

Fig. 13. Some examples of different kind of relationships between SWC measured and estimated during the June 16 event.

4.4.2 Relationship between SWC and rainfall properties

629

630 At the event time scale, SWC variations mostly depend on rainfall intensity, which varies
631 according to season, and on the initial SWC before rainfall which also varies according to land
632 covers. The reaction time (*ReacT*) is defined as the time between the beginning of rainfall and the
633 beginning of SWC increase at the sensor depth. Rising time (*RisT*) is defined as the time between
634 the start of SWC increase at the sensor depth and the moment of the peak. Amplitude (*Amp*) is
635 defined as the ratio between the SWC peak and the initial SWC value (before rainfall starts).
636 *ReacT* (Table 4) was generally shorter in grassland than in black marl and forest. In black marl, the
637 larger reactivity delay measured at the depth interval 10-20 cm can be explained by the material
638 anisotropy due to marl layer bedding and orientation, which results in shallow preferential lateral
639 subsurface flows (0 - 10cm) (Calvo-Cases *et al.*, 1991; Castillo *et al.*, 2003; Cantón *et al.*, 2011;
640 Garel *et al.*, 2012). In forest areas, water reaches the soil with a delay that depends on tree
641 canopy interception. *ReacT* observed during intense summer rainfall events was minimal in
642 grassland. In black marl, the shortest *ReacT* was observed during autumn rainfall events. *Amp*
643 dynamics in grassland and black marl were similar at the event time scale. Low *Amp* observed in
644 forest areas was due to high SWC throughout the study period. Nonetheless, very similar SWC
645 variations could be observed among all land covers during the November 24/25 rainfall event due
646 to a high mean SWC value at the catchment scale (88.6 mm cumulative rainfall during the
647 November 21/22 event). Eventually, there was a clear distinction between seasons, with shorter
648 *ReacT* and *RisT* during summer events (June 16; June 18; September 12) than during autumn
649 events (October 14; November 4/5; November 21/22; November 24/25).

650

651 **Table 4. Plot scale SWC variation at the event time scale - mean values by land cover.**

652

653 **Event Rainfall**		**SWC rate variation**	**Black marl**	**Forest**	**Grassland**
654 June 16					
655 Cumulative rainfall (mm)	31.2	Rising time (min)	65	61	35

Mean intensity (mm/h)	5.43	Increase time (min)	190	240	170
Maximum intensity (mm/h)	24.0	Amplitude (%)	23.4	16.5	33.1
June 18					
Cumulative rainfall (mm)	36.8	Rising time (min)	50	40	35
Mean intensity (mm/h)	8.66	Increase time (min)	120	100	55
Maximum intensity (mm/h)	31.2	Amplitude (%)	17.1	12.2	17.8
September 12					
Cumulative rainfall (mm)	17.8	Rising time (min)	72	68	65
Mean intensity (mm/h)	4.45	Increase time (min)	172	130	70
Maximum intensity (mm/h)	28.8	Amplitude (%)	18.6	19.1	28.7
October 14					
Cumulative rainfall (mm)	54.2	Rising time (min)	122	138	55
Mean intensity (mm/h)	2.85	Increase time (min)	155	240	215
Maximum intensity (mm/h)	40	Amplitude (%)	35.4	23.1	28.7
November 4/5					
Cumulative rainfall (mm)	46.8	Rising time (min)	235	240	210
Mean intensity (mm/h)	1.66	Increase time (min)	1040	1075	1090
Maximum intensity (mm/h)	12	Amplitude (%)	25.6	19.2	17.2
November 21/22					
Cumulative rainfall (mm)	88.6	Rising time (min)	255	287	195
Mean intensity (mm/h)	2.38	Increase time (min)	965	1100	1430
Maximum intensity (mm/h)	9.6	Amplitude (%)	19.2	11.6	16.1
November 24/25					
Cumulative rainfall (mm)	98.2	Rising time (min)	30	63	50
Mean intensity (mm/h)	2.85	Increase time (min)	130	916	85
Maximum intensity (mm/h)	12.8	Amplitude (%)	15.2	15.7	18.5

Several parameters such as the cumulative rainfall, the number of days since antecedent rainfall events, rainfall duration, rainfall mean and maximum intensity, initial SWC, *ReacT*, *RisT* and *Amp* were crossed in order to find out relationships allowing to better understand SWC dynamics at the event scale and among monitored land covers (Fig. 14). Three significant relationships emerged from this analysis. Mean rainfall intensity was inversely correlated to *ReacT* and *RisT*. High mean rainfall intensity leaded to short reaction and short rising time whatever the

land cover. An expected correlation was observed between initial SWC and *Amp*. Low initial SWC induced higher SWC variations. However, this relationship was different according to the monitored land covers: SWC variations proved lower in forest than in grassland and black marl. Moreover, initial SWC ranged from 7% to 27% in black marl, from 13% to 32% in grassland, and from 22% to 41% in forest. From these observations, it can be concluded that soils under forest have a greater storage capacity (higher porosity) but drainage is better in soils under grassland (higher transmissivity).

Fig. 14. Three significant relationships between rainfall properties and some SWC index (initial SWC, variation amplitude) at the plot scale and the event time scale.

4.4.3 Subsurface flow processes

98 *Smax* values were computed from the seven studied flood events (Fig. 15). Low *Smax* (< 1000) represented 45% of measured *Smax* and were mainly associated to November events. The frequency of low *Smax* increased from the beginning to the end of November according to the catchment wetting. Low *Smax* were almost equally observed in every monitored land cover with a higher number of observations in forest due to a higher number of monitored plots (6 against 4 in black marl and 4 in grassland). The frequency of *Smax* between 1000 and 5000 was lower in forest and black marl than in grassland. High *Smax* (> 5000) were only measured during summer events and during the first fall event (October 14). *Smax* > 6000 were mainly measured in grassland.

Relationships between *Smax*, land cover and initial SWC are consistent with observations made in Fig. 4. High *Smax* were more often observed in grassland where the probes reacted more quickly to rainfall due to higher transmissivity of soils and to the limited impact of interception.

Conversely, low *Smax* were predominant in forest due to lower drainage capacity and high interception by trees. *Smax* observed in black marl were similar to the *Smax* in the forest although isolated observations of very high *Smax* were observed. Occurrence of subsurface flow in black marl is explained by the anisotropic nature of the material involving preferential lateral flow.

Fig. 15. Frequency distribution of *Smax* calculated from all sensors at 15 cm depth. Left graph shows *Smax* frequency distribution by land cover. Right graph shows *Smax* frequency distribution by event.

5 Discussions

5.1 Remarks on SWC measurements

Detailed knowledge of SWC absolute values over the catchment would require a network of numerous probes that would entail high costs to install and to maintain in good conditions. Finally, a capacitance sensor network composed of a small number of low cost probes was suitable for studying SWC mean variation at daily, hourly and event time scales in the Laval catchment. This is supported by recent findings of Mälicke *et al.* (2020) who demonstrated (from a study in the 19.4 km² Colpach catchment) that a minimal number of SWC sensors could capture soil moisture dynamics at the catchment scale and explain its hydrological dynamic. Sensors location strategy is a key point in the purpose of estimating soil moisture mean status at the catchment scale. This strategy is usually based on identified soil-landscape units using different geostatistical methodologies (Corradini, 2014 ; Zhuo *et al*., 2020). Backing up the existing probe network with other sensors to monitor SWC in the identified soil-landscape units elsewhere in the catchment could enhance the proposed methodology by validating mean porosity values measured among land covers to characterize SWC more accurately. Eventually, *Smax* analysis

741 would have been enhanced if SWC data obtained by the same sensors at multiple depths were
742 available.
743
744 Extreme SWC values (dry or wet) are a key point impacting soil water exchanges (Teuling *et*
745 *al.*, 2006). Mittlebach *et al.* (2011) showed that accuracy measurement of 10HS sensor decreases
746 with increased SWC, which results in overestimation at low SWC and underestimation at high
747 SWC (> 40%) especially in clay soils. Extreme SWC values measured by 10HS in the Laval
748 catchment (values corrected by field-calibration) were near 0% but never exceeded 40% in black
749 marl, whereas they were never less than 12% and regularly exceeded 40% in forest and grassland
750 at the event time scale. It is well known that SWC capacitance sensor accuracy depends on the
751 effect of the monitored soil properties on site-specific calibration. On this basis, a specific effort
752 must be made to reduce measurement errors, especially for extreme high values. Mittlebach *et*
753 *al.* (2011) showed that specific site-calibration of the 10HS sensor can help reduce measurement
754 error to 2% (with error values ranging from -7% to 3% in loamy soils and from -8% to 5% in clayey
755 soils). In the Laval catchment, the forest field-site calibration was similar to the manufacturer's
756 calibration, whereas the field-site calibration was different in grassland and black marl. The field-
757 site calibration reduced the 10HS sensor mean measurement error from 12% to 3% in grassland
758 and from 11% to 4% in black marl. It is assumed that a 4% mean measurement error is reasonable
759 for estimating mean SWC patterns at the catchment scale. Moreover, estimated SWC values in
760 the investigated and validation plots were primarily less than measurement error.
761
762 **5.2 Explanatory variables and SWC estimation**
763
764 The five variables used in the geostatistical model were appropriate for estimating SWC at
765 the catchment scale. Regarding relationships between some of these variables, questions about
766 the impact of each variable in the geostatistical model could be asked. What impact if only NDVI

767 and soil depth were used to run the model? Different combinations from 2 to 5 variables were
768 tested. The difference in estimated SWC using two variables (mean R^2 = 0.84) and five variables
769 (R^2 = 0.88) was very low. But except for curvature index, each variable enhanced the SWC
770 estimation during rainfall periods. However, these variables give a simplified understanding of
771 SWC variation at the catchment scale. Using soil properties could help explain SWC variation at
772 the event time scale. Indeed, regolith type, thickness, dip orientation, porosity, and soil infiltration
773 capacity are parameters that affect SWC and runoff generation at the hillslope scale, which
774 contribute to the hydrological complexity of badlands (Kuhn *et al.*, 2004). But at present time it
775 was not possible to properly map these data.
776
777 Finally, model uncertainties can be attributed to the low number of measurement plots
778 and the high natural heterogeneity of SWC in a mountainous and steep environment. Even if the
779 model takes into account local variables that affect SWC at the plot scale, estimated values at
780 unmeasured plots are influenced by SWC values of the nearest measured plots (Lhottelier, 2006).
781
782 **5.3 Impact of the catchment hydric status, geomorphology and landuse on SWC-runoff thresholds and**
783 **SWC space-time variability**
784
785 In dry period, peakflow measured in the Laval resulted mainly from hortonian runoff and
786 occurred before peak SWC. In wet period, higher subsurface flow occurrence resulted in an earlier
787 reaction of SWC than streamflow. These delays between max SWC and peakflow are similar to
788 what Penna *et al.* (2011) observed in the 1.9 km² moutainous Rio Vauz catchment (elevations
789 ranging from 1835 m to 3152 m) mainly composed of Dolomitic rock cliffs, steep slopes and a
790 valley bottom covered by Quaternary till. These results highlight a reproducibility of soil
791 hydrological processes despite various land uses and geomorphology. At the seasonal scale, Fan
792 *et. al* (2020) observed in a 0.08 km² forested catchment in Pennsylvania (USA) dominated by a

humid continental climate that SWC was spatially more variable but temporally more stable during wet cold season compared to dry warm season. Observations made in the Laval are different since the Mediterranean climate is very contrasted with a long dry period with rare, short and intense storms while the wet period has a temporally heterogeneous distribution of long and high cumulative rainfalls. Recharge and drainage phases are then easily identified regarding to SWC spatial and temporal dynamic.

In terms of hillslope morphology, Moore *et al.* (1998) observed in a 0.075 km² gully catchment located in New South Wales (Australia) that topographic nonuniformity within small catchments controlled SWC spatial variability and the location of ephemeral gullies. They showed that dry near-surface soils were quite propitious to gullies development. Similar observations were made in the Laval catchment which also has a very dense gully network located on bare areas (Thommeret, 2012). In the Laval the deepest and most durable gullies are located at the bottom of concave hillslopes where near-surface SWC is greater than SWC measured at upslope and mid-slope areas which are more propitious to ephemeral gullies whatever the slope shape. In a 0.56 km² agricultural (essentially wheat) and semi-arid catchment located in Eastern Colorado (USA), Green and Erskine (2011) showed that vertical processes appeared to control SWC profile dynamics at summit positions while infrequent overland flow and unsaturated subsurface lateral flow appeared to control SWC dynamics at downslope positions. Subsurface lateral flow type is also dominant downslope in the Laval catchment whatever the land use. However, situations is quite different at summit and mid-slope in black marl areas regarding to the variability of soil hydraulic conductivity values, material anisotropy and rainfall intensity (Estèves *et al.*, 2005). Thus, summit are more associated to overland flow type while water is transported from summit to hillslope bottom by a combination of overland and lateral subsurface flow processes.

6 Conclusions and outlook

This study showed that mean SWC dynamics can be related to specific soil-vegetation patterns in badlands and that it is possible to distinguish SWC signatures among land covers. Geostatistical modeling using a small number of geographical variables makes it possible to estimate SWC at the plot scale and at daily and hourly time steps. These geographical variables are useful to predict wetness/dryness status at the catchment scale apart from flash flood events. However, it is not possible to determine the impact of these variables on the studied land covers separately. At the event scale, SWC dynamic analysis (*Smax* index) made it possible to show that matrix flow would be associated to long autumn rainfall with low intensity producing low outflow (Qmax < 1500 l/s) and would appear in every land covers (Fig. 16). While preferential flows would be caused by summer storm with high rainfall intensity giving birth to large flood such as the October 14 event (Qmax = 10 000 l/s) and would be more often observed in grassland.

Fig. 16. Relationships between SWC measurement time steps, variables determining SWC, hydrological processes and land covers.

Future work will focus on validating this methodology by modeling hydrological processes with a physically-based model that integrates climate forcing especially on surface runoff. Regarding to high SWC variations it is assumed that black marls area have a major contribution to stream flows whereas water stored in grassland and especially in forests where soils are deeper is primarily lost for runoff. The goal of the future work will be to assess independently the impact of the areal distribution of SWC on runoff generation.

7 Acknowledgments

This work was supported by the Provence-Alpes-Côte-d'Azur region (OCTOMED project fund) and the ORE Draix-Bléone. It was also supported by public funds received in the framework of GEOSUD, a project (ANR-10-EQPX-20) of the program "Investissements d'Avenir" managed by the French National Research Agency.

References

A

Abdelli, F., Ouessar, M., M'Hemdi, S., Guied, M., Khatteli, H., 2017. Monitoring Soil Moisture Content of Jessour in the Watershed of Wadi Jir (Matmata, Southeast Tunisia), in: Water and Land Security in Drylands. Springer, Cham, pp. 97–110. https://doi.org/10.1007/978-3-319-54021-4_10

Altdorff, D., Hebel, C. von, Borchard, N., Kruk, J. van der, Bogena, H.R., Vereecken, H., Huisman, J.A., 2017. Potential of catchment-wide soil water content prediction using electromagnetic induction in a forest ecosystem. Environ Earth Sci 76, 111. https://doi.org/10.1007/s12665-016-6361-3

Arnaud, M., Emery, X., 2000. Estimation et interpolation spatiale : méthodes déterministes et méthodes géostatistiques [WWW Document]. URL http://agritrop.cirad.fr/487412/ (accessed 1.1.18).

B

Baghdadi, N., Grandjean, G., Lahondère, D., Paillou, P., Lasne, Y., 2005. Apport de l'imagerie satellitaire radar pour l'exploration géologique en zones arides. Comptes Rendus Geoscience 337, 719–728. https://doi.org/10.1016/j.crte.2005.03.003

Bárdossy, A., Lehmann, W., 1998. Spatial distribution of soil moisture in a small catchment. Part 1: geostatistical analysis. Journal of Hydrology 206, 1–15. https://doi.org/10.1016/S0022-1694(97)00152-2

874 Beven, K.J., 2000. Uniqueness of place and process representations in hydrological modelling. Hydrology and Earth System
875 Sciences 4, 203–213. https://doi.org/10.5194/hess-4-203-2000
876 Biswas, A., Si, B.C., 2011. Identifying scale specific controls of soil water storage in a hummocky landscape using wavelet
877 coherency. Geoderma 165, 50–59. https://doi.org/10.1016/j.geoderma.2011.07.002
878 Blonquist, J.M., Jones, S.B., Robinson, D.A., 2005. Standardizing Characterization of Electromagnetic Water Content Sensors.
879 Vadose Zone Journal 4, 1059–1069. https://doi.org/10.2136/vzj2004.0141
880 Blume, T., Zehe, E., Bronstert, A., 2009. Use of soil moisture dynamics and patterns at different spatio-temporal scales for
881 the investigation of subsurface flow processes. Hydrol. Earth Syst. Sci. 13, 1215–1233. https://doi.org/10.5194/hess-13-
882 1215-2009
883 Blyth, E.M., Finch, J., Robinson, M., Rosier, P., 2004. Can soil moisture be mapped onto the terrain? Hydrology and Earth
884 System Sciences Discussions 8, 923–930.
885 Bogena, H.R., Herbst, M., Huisman, J.A., Rosenbaum, U., Weuthen, A., Vereecken, H., 2010. Potential of Wireless Sensor
886 Networks for Measuring Soil Water Content Variability. Vadose Zone Journal 9, 1002–1013.
887 https://doi.org/10.2136/vzj2009.0173
888 Bogena, H.R., Huisman, J.A., Baatz, R., Hendricks Franssen, H.-J., Vereecken, H., 2013. Accuracy of the cosmic-ray soil water
889 content probe in humid forest ecosystems: The worst case scenario. Water Resour. Res. 49, 5778–5791.
890 https://doi.org/10.1002/wrcr.20463
891 Borges, A.L., 1993. Modélisation de l'érosion sur deux bassins versants expérimentaux des Alpes du Sud (phdthesis).
892 Université Joseph-Fourier - Grenoble I.
893 Braud, I., Desprats, J.-F., Ayral, P.-A., Bouvier, C., & Vandervaere, J.-P. (2017). Mapping topsoil field-saturated hydraulic
894 conductivity from point measurements using different methods. Journal of Hydrology and Hydromechanics, 65(3), 264-
895 275. https://doi.org/10.1515/johh-2017-0017
896 Brevik, E.C., Fenton, T.E., Lazari, A., 2006. Soil electrical conductivity as a function of soil water content and implications for
897 soil mapping. Precision Agric 7, 393–404. https://doi.org/10.1007/s11119-006-9021-x
898 Brillante, L., Bois, B., Mathieu, O., Bichet, V., Michot, D., Lévêque, J., 2014. Monitoring soil volume wetness in
899 heterogeneous soils by electrical resistivity. A field-based pedotransfer function. Journal of Hydrology, Determination of
900 soil moisture: Measurements and theoretical approaches 516, 56–66. https://doi.org/10.1016/j.jhydrol.2014.01.052
901 Brocca, L., Melone, F., Moramarco, T., Morbidelli, R., 2010. Spatial-temporal variability of soil moisture and its estimation
902 across scales. Water Resour. Res. 46, W02516. https://doi.org/10.1029/2009WR008016
903 Brocca, L., Tullo, T., Melone, F., Moramarco, T., Morbidelli, R., 2012. Catchment scale soil moisture spatial–temporal
904 variability. Journal of Hydrology 422, 63–75. https://doi.org/10.1016/j.jhydrol.2011.12.039

Broedel, E., Tomasella, J., Cândido, L.A., von Randow, C., 2017. Deep soil water dynamics in an undisturbed primary forest in central Amazonia: Differences between normal years and the 2005 drought. Hydrol. Process. 31, 1749–1759. https://doi.org/10.1002/hyp.11143

Brunet, P., Clément, R., Bouvier, C., 2010. Monitoring soil water content and deficit using Electrical Resistivity Tomography (ERT) - A case study in the Cevennes area, France. Journal of Hydrology, 380(1): 146-153. DOI:10.1016/j.jhydrol.2009.10.032

Burrough, T. late P.P.A., McDonnell, R.A., Lloyd, C.D., 2015. Principles of Geographical Information Systems, Third Edition. ed. Oxford University Press, Oxford, New York.

C

Calamita, G., Perrone, A., Brocca, L., Onorati, B., Manfreda, S., 2015. Field test of a multi-frequency electromagnetic induction sensor for soil moisture monitoring in southern Italy test sites. Journal of Hydrology 529, 316–329. https://doi.org/10.1016/j.jhydrol.2015.07.023

Calvo-Cases, A., Harvey, A.M., Paya-Serrano, J., Alexander, R.W., 1991. Response of badland surfaces in south east Spain to simulated rainfall. Cuaternario y Geomorfologia, 5, 3-14

Cantón, Y., Solé-Benet, A., de Vente, J., Boix-Fayos, C., Calvo-Cases, A., Asensio, C., Puigdefábregas, J., 2011. A review of runoff generation and soil erosion across scales in semiarid south-eastern Spain. Journal of Arid Environments, Deserts of the World Part IV: Iberian Southeast 75, 1254–1261. https://doi.org/10.1016/j.jaridenv.2011.03.004

Cao, D., Shi, B., Zhu, H., Zhu, K., Wei, G., Gu, K., 2016. Performance evaluation of two types of heated cables for distributed temperature sensing-based measurement of soil moisture content. Journal of Rock Mechanics and Geotechnical Engineering 8, 212–217. https://doi.org/10.1016/j.jrmge.2015.09.005

Castillo, V.M., Gómez-Plaza, A., Martínez-Mena, M., 2003. The role of antecedent soil water content in the runoff response of semiarid catchments: a simulation approach. Journal of Hydrology 284, 114–130. https://doi.org/10.1016/S0022-1694(03)00264-6

Comegna, V., Basile, A., 1994. Temporal stability of spatial patterns of soil water storage in a cultivated Vesuvian soil. Geoderma 62, 299–310. https://doi.org/10.1016/0016-7061(94)90042-6

Corradini, C. 2014. Soil moisture in the development of hydrological processes and its determination at different spatial scales. Journal of Hydrology. doi:10.1016/j.jhydrol.2014.02.051.

Corrao, M.V., Link, T.E., Heinse, R., Eitel, J.U.H., 2017. Modeling of terracette-hillslope soil moisture as a function of aspect, slope and vegetation in a semi-arid environment. Earth Surface Processes and Landforms 42, 1560–1572. https://doi.org/10.1002/esp.4114

Cosandey, C., Andréassian, V., Martin, C., Didon-Lescot, J.F., Lavabre, J., Folton, N., Mathys, N., Richard, D., 2005. The hydrological impact of the mediterranean forest: a review of French research. Journal of Hydrology 301, 235–249. https://doi.org/10.1016/j.jhydrol.2004.06.040

Cras, A., Marc, V., Travi, Y., 2007. Hydrological behaviour of sub-Mediterranean alpine headwater streams in a badlands environment. Journal of Hydrology 339, 130–144. https://doi.org/10.1016/j.jhydrol.2007.03.004

D

De Lannoy, G.J.M., Verhoest, N.E.C., Houser, P.R., Gish, T.J., Van Meirvenne, M., 2006. Spatial and temporal characteristics of soil moisture in an intensively monitored agricultural field (OPE3). Journal of Hydrology 331, 719–730. https://doi.org/10.1016/j.jhydrol.2006.06.016

Dehotin, J., Braud, I., 2008. Which spatial discretization for distributed hydrological models? Proposition of a methodology and illustration for medium to large-scale catchments. Hydrol. Earth Syst. Sci. 12, 769–796. https://doi.org/10.5194/hess-12-769-2008

Descroix, L., Mathys, N., 2003. Processes, spatio-temporal factors and measurements of current erosion in the French Southern Alps: a review. Earth Surf. Process. Landforms 28, 993–1011. https://doi.org/10.1002/esp.514

Dobriyal, P., Qureshi, A., Badola, R., Hussain, S.A., 2012. A review of the methods available for estimating soil moisture and its implications for water resource management. Journal of Hydrology s 458–459, 110–117. https://doi.org/10.1016/j.jhydrol.2012.06.021

Douvinet, J., 2008. Les bassins versants sensibles aux “crues rapides” dans le Bassin Parisien : Analyse de la structure et de la dynamique des systèmes spatiaux complexes (thesis). Caen.

Douvinet, J., Van De Wiel, M.J., Delahaye, D., Cossart, E., 2015. A flash flood hazard assessment in dry valleys (northern France) by cellular automata modelling. Nat Hazards 75, 2905–2929. https://doi.org/10.1007/s11069-014-1470-3

Dubreuil-Boisclair, C., Gloaguen, E., Marcotte, D., Giroux, B., 2011. Heterogeneous aquifer characterization from ground-penetrating radar tomography and borehole hydrogeophysical data using nonlinear Bayesian simulations. GEOPHYSICS 76, J13–J25. https://doi.org/10.1190/1.3571273

E

El Hajj, M., Baghdadi, N., Zribi, M., Bazzi, H., 2017. Synergic Use of Sentinel-1 and Sentinel-2 Images for Operational Soil Moisture Mapping at High Spatial Resolution over Agricultural Areas. Remote Sensing 9, 1292. https://doi.org/10.3390/rs9121292

Esteves, M., Descroix, L., Mathys, N., Marc Lapetite, J., 2005. Soil hydraulic properties in a marly gully catchment (Draix, France). CATENA 63, 282–298. https://doi.org/10.1016/j.catena.2005.06.006

F

Fan, B., Tao, W., Qin, G., Hopkins, I., Zhang, Y., Wang, Q., Lin, H., & Guo, L. (2020). Soil micro-climate variation in relation to slope aspect, position, and curvature in a forested catchment. Agricultural and Forest Meteorology, 290, 107999. https://doi.org/10.1016/j.agrformet.2020.107999

G

Gallart, F., Marignani, M., Pérez-Gallego, N., Santi, E., Maccherini, S., 2013. Thirty years of studies on badlands, from physical to vegetational approaches. A succinct review. CATENA, Updating Badlands Research 106, 4–11. https://doi.org/10.1016/j.catena.2012.02.008

Garel, E., Marc, V., Ruy, S., Cognard-Plancq, A.-L., Klotz, S., Emblanch, C., Simler, R., 2012. Large scale rainfall simulation to investigate infiltration processes in a small landslide under dry initial conditions: the Draix hillslope experiment. Hydrol. Process. 26, 2171–2186. https://doi.org/10.1002/hyp.9273

Gratton, Y., 2002. Le krigeage: la méthode optimale d'interpolation spatiale. Les articles de l'Institut d'Analyse Géographique.

Grayson, R.B., Western, A.W., 1998. Towards areal estimation of soil water content from point measurements: time and space stability of mean response. Journal of Hydrology 207, 68–82. https://doi.org/10.1016/S0022-1694(98)00096-1

Green, T.R., Erskine, R.H., 2011. Measurement and inference of profile soil-water dynamics at different hillslope positions in a semiarid agricultural watershed. Water Resources Research 47. https://doi.org/10.1029/2010WR010074

H

Hengl T., Heuvelink G., Rossiter D.G., 2007. About regression-kriging: From equations to case studies. Computers & Geosciences, 33(10): 1301-1315. doi :10.1016/j.cageo.2007.05.001

Hocking, R. R. (1976). A biometrics invited paper. The analysis and selection of variables in linear regression. Biometrics, 32(1), 1e49. http://dx.doi.org/10.2307/2529336.

Hapuarachchi, H. a. P., Wang, Q.J., Pagano, T.C., 2011. A review of advances in flash flood forecasting. Hydrol. Process. 25, 2771–2784. https://doi.org/10.1002/hyp.8040

Hoef, J.M.V., Cressie, N., 1993. Multivariable spatial prediction. Math Geol 25, 219–240. https://doi.org/10.1007/BF00893273

Hu, W., Shao, M., Han, F., Reichardt, K., Tan, J., 2010. Watershed scale temporal stability of soil water content. Geoderma 158, 181–198. https://doi.org/10.1016/j.geoderma.2010.04.030

Huisman, J.A., Hubbard, S.S., Redman, J.D., Annan, A.P., 2003. Measuring Soil Water Content with Ground Penetrating Radar. Vadose Zone Journal 2, 476–491. https://doi.org/10.2136/vzj2003.4760

J

Jawson, S.D., Niemann, J.D., 2007. Spatial patterns from EOF analysis of soil moisture at a large scale and their dependence on soil, land-use, and topographic properties. Advances in Water Resources 30, 366–381. https://doi.org/10.1016/j.advwatres.2006.05.006

Joly, D., Brossard, T., Cardot, H., Cavailhes, J., Hilal, M., Wavresky, P., 2008. Interpolation par recherche d'information locale. Interpolation by local information 27–47. https://doi.org/https://doi.org/10.4267/climatologie.714

Joly D., Brossard T., Cardot H., Cavailhès J., Hilal M., Wavresky P., 2010. Les types de climats en France, une construction spatiale (Types of climate on continental France, a spatial construction). Cybergeo: European Journal of Geography, 501. URL : http://cybergeo.revues.org/23155 ; DOI : 10.4000/cybergeo.23155

Joly D., Brossard T., Cardot H., Cavailhès J., Hilal M., Wavresky P., 2011. Temperature Interpolation by local information; the example of France. International Journal of Climatology, 31(14): 2141-2153.

Jones, S.B., Blonquist, J.M., Robinson, D.A., Philip Rasmussen, V., 2005. Standardizing characterization of electromagnetic water content sensors: Part 1. Methodology. Vadose Zone Journal. SSSA: 1048-1058

K

Kachanoski, R.G., Wesenbeeck, I.J.V., Gregorich, E.G., 1988. Estimating Spatial Variations of Soil Water Content Using Noncontacting Electromagnetic Inductive Methods. Can. J. Soil. Sci. 68, 715–722. https://doi.org/10.4141/cjss88-069

Kachanoski, R.G., Wesenbeeck, I.J.V., Jong, E.D., 1990. Field Scale Patterns of Soil Water Storage from Non-Contacting Measurements of Bulk Electrical Conductivity. Can. J. Soil. Sci. 70, 537–542. https://doi.org/10.4141/cjss90-056

Köhli, M., Schrön, M., Zreda, M., Schmidt, U., Dietrich, P., Zacharias, S., 2015. Footprint characteristics revised for field-scale soil moisture monitoring with cosmic-ray neutrons. Water Resour. Res. 51, 5772–5790. https://doi.org/10.1002/2015WR017169

Krzeminska, D.M., Steele-Dunne, S.C., Bogaard, T.A., Rutten, M.M., Sailhac, P., Geraud, Y., 2012. High-resolution temperature observations to monitor soil thermal properties as a proxy for soil moisture condition in clay-shale landslide. Hydrol. Process. 26, 2143–2156. https://doi.org/10.1002/hyp.7980

Kuhn, N.J., Yair, A., 2004. Spatial distribution of surface conditions and runoff generation in small arid watersheds, Zin Valley Badlands, Israel. Geomorphology 57, 183–200. https://doi.org/10.1016/S0169-555X(03)00102-8

L

Langlois P., Delahaye D., 2002. RuiCells, automate cellulaire pour la simulation du ruissellement de surface. Revue internationale de géomatique, vol 12, n°4, P461-487. Doi:10.3166/rig.12.461-487

Le Barbu, E., 2006. Modélisation pluie-débit érosion sur un bassin versant expérimental des Alpes du Sud. Rapport de stage 2° année ingénieur Thesis, ENTPE, Lyon, 85p

Lhotellier, R., 2006. Spatialisation de la température minimale de l'air à échelle quotidienne sur quatre départements alpins français. Spatialization of daily minimum air temperature on four French alpine departments 55–69. https://doi.org/https://doi.org/10.4267/climatologie.695

Liu, X., Luo, T., 2011. Spatiotemporal Variability of Soil Temperature and Moisture across two Contrasting Timberline Ecotones in the Sergyemla Mountains, Southeast Tibet. Arctic, Antarctic, and Alpine Research 43, 229–238. https://doi.org/10.1657/1938-4246-43.2.229

Lozano-Parra, J., Schaik, N.L.M.B. van, Schnabel, S., Gómez-Gutiérrez, Á., 2016. Soil moisture dynamics at high temporal resolution in a semiarid Mediterranean watershed with scattered tree cover. Hydrological Processes 30, 1155–1170. https://doi.org/10.1002/hyp.10694

M

1056 Malet, J.-P., Asch, T.W.J.V., Beek, R.V., Maquaire, O., 2005. Forecasting the behaviour of complex landslides with a spatially
1057 distributed hydrological model. Natural Hazards and Earth System Science 5, 71–85.
1058 Mälicke, M., Hassler, S.K., Blume, T., Weiler, M., Zehe, E., 2020. Soil moisture: variable in space but redundant in time.
1059 Hydrology and Earth System Sciences 24, 2633–2653. https://doi.org/10.5194/hess-24-2633-2020
1060 Mallet, F., Carrière, S.D., Chalikakis, K., Marc, V., 2018. Assessing soil water content spatio-temporal variability at the
1061 hillslope scale in a headwater catchment using a multi variable interpolation model based on EMI surveys (Draix, South
1062 Alps, France). Environ Earth Sci 77, 507. https://doi.org/10.1007/s12665-018-7687-9
1063 Mallet, F., 2018. Spatialisation et modélisation de l'état hydrique des sols pour l'étude des processus de formation des
1064 écoulements en contexte torrentiel : application au bassin versant marneux du Laval (ORE Draix-Bléone, Alpes-De-
1065 Haute-Provence, France) (phdthesis). Université d'Avignon.
1066 Maquaire, O., Ritzenthaler, A., Fabre, D., Ambroise, B., Thiery, Y., Truchet, E., Malet, J.-P., Monnet, J., 2002. Caractérisation
1067 des profils de formations superficielles par pénétrométrie dynamique à énergie variable : application aux marnes noires
1068 de Draix (Alpes-de-Haute-Provence, France). Comptes Rendus Geoscience 334, 835–841.
1069 https://doi.org/10.1016/S1631-0713(02)01788-1
1070 Martini, E., Werban, U., Zacharias, S., Pohle, M., Dietrich, P., Wollschläger, U., 2017. Repeated electromagnetic induction
1071 measurements for mapping soil moisture at the field scale: validation with data from a wireless soil moisture
1072 monitoring network. Hydrol. Earth Syst. Sci. 21, 495–513. https://doi.org/10.5194/hess-21-495-2017
1073 Matheron, G., 1970. Random Functions and their Application in Geology, in: Geostatistics, Computer Applications in the
1074 Earth Sciences. Springer, Boston, MA, pp. 79–87. https://doi.org/10.1007/978-1-4615-7103-2_7
1075 Mathys, N., Brochot, S., Meunier, M., Richard, D., 2003. Erosion quantification in the small marly experimental catchments
1076 of Draix (Alpes de Haute Provence, France). Calibration of the ETC rainfall–runoff–erosion model. CATENA, Gully Erosion
1077 and Global Change 50, 527–548. https://doi.org/10.1016/S0341-8162(02)00122-4
1078 Mathys, N., Klotz, S., Esteves, M., Descroix, L., Lapetite, J.M., 2005. Runoff and erosion in the Black Marls of the French Alps:
1079 Observations and measurements at the plot scale. CATENA, Gully Erosion: A Global Issue 63, 261–281.
1080 https://doi.org/10.1016/j.catena.2005.06.010
1081 Mathys, N., 2006. Analyse et modélisation à différentes échelles des mécanismes d'érosion et de transport de matériaux
1082 solides. Cas des petits bassins versants de montagne sur marne (Draix, Alpes-de-Haute-Provence). Thèse de doctorat,
1083 Institut National Polytechnique de Grenoble, 339 p
1084 Meerveld, H.J.T., McDonnell, J.J., 2006. Threshold relations in subsurface stormflow: 2. The fill and spill hypothesis. Water
1085 Resources Research 42. https://doi.org/10.1029/2004WR003800

Michot, D., Benderitter, Y., Dorigny, A., Nicoullaud, B., King, D., Tabbagh, A., 2003. Spatial and temporal monitoring of soil water content with an irrigated corn crop cover using surface electrical resistivity tomography. Water Resour. Res. 39, 1138. https://doi.org/10.1029/2002WR001581

Mittelbach, H., Casini, F., Lehner, I., Teuling, A.J., Seneviratne, S.I., 2011. Soil moisture monitoring for climate research: Evaluation of a low-cost sensor in the framework of the Swiss Soil Moisture Experiment (SwissSMEX) campaign. J. Geophys. Res. 116, D05111. https://doi.org/10.1029/2010JD014907

Mohanty, B.P., Skaggs, T.H., 2001. Spatio-temporal evolution and time-stable characteristics of soil moisture within remote sensing footprints with varying soil, slope, and vegetation. Advances in Water Resources, Nonlinear Propagation of Multi-scale Dynamics Through Hydrologic Subsystems 24, 1051–1067. https://doi.org/10.1016/S0309-1708(01)00034-3

Moore, I.D., Burch, G.J., Mackenzie, D.H., 1998. Topographic Effects on the Distribution of Surface Soil Water and the Location of Ephemeral Gullies [WWW Document], n.d. URL https://doi.org/10.13031/2013.30829 (accessed 7.21.20).

N

Ni, J., Cheng, Y., Wang, Q., Ng, C.W.W., Garg, A., 2019. Effects of vegetation on soil temperature and water content: Field monitoring and numerical modelling. Journal of Hydrology 571, 494–502. https://doi.org/10.1016/j.jhydrol.2019.02.009

O

Ocampo, C.J., Sivapalan, M., Oldham, C., 2006. Hydrological connectivity of upland-riparian zones in agricultural catchments: Implications for runoff generation and nitrate transport. Journal of Hydrology 331, 643–658. https://doi.org/10.1016/j.jhydrol.2006.06.010

Ochsner, T.E., Cosh, M.H., Cuenca, R.H., Dorigo, W.A., Draper, C.S., Hagimoto, Y., Kerr, Y.H., Njoku, E.G., Small, E.E., Zreda, M., Larson, K.M., 2013. State of the Art in Large-Scale Soil Moisture Monitoring. Soil Science Society of America Journal 77, 1888–1919. https://doi.org/10.2136/sssaj2013.03.0093

P

Panissod, F., Bailly, J-S, Durrieu, S., Jacome, A., Mathys, N., Cavalli, M., Puech, C., 2010. Qualification de modèles numériques de terrain LiDAR pour l'érosion : application aux badlands de Draix. Revue Française de Photogrammétrie et de Télédétection, volume 192, 50-57.

Penna, Daniele; Tromp-van Meerveld, H J; Gobbi, Alberto; Borga, Marco; Dalla Fontana, Giancarlo (2011). The influence of soil moisture on threshold runoff generation processes in an alpine headwater catchment. Hydrology and Earth System Sciences, 15(3):689-702.

Penna, D., Brocca, L., Borga, M., & Dalla Fontana, G. (2013). Soil moisture temporal stability at different depths on two alpine hillslopes during wet and dry periods. Journal of Hydrology, 477, 55-71. https://doi.org/10.1016/j.jhydrol.2012.10.052

Plutowski, M., Sakata, S., & White, H. (1994). Cross-validation estimates IMSE. In J. D. Cowan, G. Tesauro, & J. Alspector (Eds.), Advances in neural information processing systems (Vol. 6, pp. 391e398). San Mateo, CA: Morgan Kaufman Publishers.

Q

Qu, W., Bogena, H.R., Huisman, J.A., Vereecken, H., 2013. Calibration of a Novel Low-Cost Soil Water Content Sensor Based on a Ring Oscillator. Vadose Zone Journal 12. https://doi.org/10.2136/vzj2012.0139

Quinn, P.F., Beven, K.J., 1993. Spatial and temporal predictions of soil moisture dynamics, runoff, variable source areas and evapotranspiration for plynlimon, mid-wales. Hydrol. Process. 7, 425–448. https://doi.org/10.1002/hyp.3360070407

R

Regüés, D., Gallart, F., 2004. Seasonal patterns of runoff and erosion responses to simulated rainfall in a badland area in Mediterranean mountain conditions (Vallcebre, southeastern Pyrenees). Earth Surf. Process. Landforms 29, 755–767. https://doi.org/10.1002/esp.1067

Robinson, D.A., Campbell, C.S., Hopmans, J.W., Hornbuckle, B.K., Jones, S.B., Knight, R., Ogden, F., Selker, J., Wendroth, O., 2008. Soil Moisture Measurement for Ecological And Hydrological Watershed-Scale Observatories: A Review. Vadose Zone J. 358–389.

Rodriguez-Iturbe, I., 2000. Ecohydrology: A hydrologic perspective of climate-soil-vegetation dynamics. Water Resources Research 36, 3–9. https://doi.org/10.1029/1999WR900210

Romano, N., 2014. Soil moisture at local scale: Measurements and simulations. Journal of Hydrology, Determination of soil moisture: Measurements and theoretical approaches 516, 6–20. https://doi.org/10.1016/j.jhydrol.2014.01.026

S

Selker, J.S., Thévenaz, L., Huwald, H., Mallet, A., Luxemburg, W., van de Giesen, N., Stejskal, M., Zeman, J., Westhoff, M., Parlange, M.B., 2006. Distributed fiber-optic temperature sensing for hydrologic systems. Water Resour. Res. 42, W12202. https://doi.org/10.1029/2006WR005326

Sidle, R.C., Tsuboyama, Y., Noguchi, S., Hosoda, I., Fujieda, M., Shimizu, T., 2000. Stormflow generation in steep forested headwaters: a linked hydrogeomorphic paradigm. Hydrol. Process. 14, 17. https://doi.org/10.1002/(SICI)1099-1085(20000228)14:3<369::AID-HYP943>3.0.CO;2-P

Sivapalan, M., 2003. Process complexity at hillslope scale, process simplicity at the watershed scale: is there a connection? Hydrological Processes 17, 1037–1041. https://doi.org/10.1002/hyp.5109

Stevens, J.T., Boisramé, G.F.S., Rakhmatulina, E., Thompson, S.E., Collins, B.M., Stephens, S.L., 2020. Forest Vegetation Change and Its Impacts on Soil Water Following 47 Years of Managed Wildfire. Ecosystems. https://doi.org/10.1007/s10021-020-00489-5

Strahler, A.N., 1952. HYPSOMETRIC (AREA-ALTITUDE) ANALYSIS OF EROSIONAL TOPOGRAPHY. GSA Bulletin 63, 1117–1142. https://doi.org/10.1130/0016-7606(1952)63[1117:HAAOET]2.0.CO;2

T

Teuling, A.J., Seneviratne, S.I., Williams, C., Troch, P.A., 2006. Observed timescales of evapotranspiration response to soil moisture. Geophys. Res. Lett. 33, L23403. https://doi.org/10.1029/2006GL028178

Thommeret, N., 2012. Analyse spatiale de réseaux de ravines hiérarchisées à partir de MNT à différentes résolutions : application aux “badlands” de Draix (Alpes-de-Haute-Provence) (These de doctorat). Paris 1.

Topp, G.C., Davis, J.L., Annan, A.P., 1980. Electromagnetic determination of soil water content: Measurements in coaxial transmission lines. Water Resour. Res. 16, 574–582. https://doi.org/10.1029/WR016i003p00574

Tramblay, Y., Bouvier, C., Martin, C., Didon-Lescot, J.-F., Todorovik, D., Domergue, J.-M., 2010. Assessment of initial soil moisture conditions for event-based rainfall–runoff modelling. Journal of Hydrology 387, 176–187. https://doi.org/10.1016/j.jhydrol.2010.04.006

Tromp-van Meerveld, H.J., McDonnell, J.J., 2009. Assessment of multi-frequency electromagnetic induction for determining soil moisture patterns at the hillslope scale. Journal of Hydrology 368, 56–67. https://doi.org/10.1016/j.jhydrol.2009.01.037

Tromp-van Meerveld, H.J., McDonnell, J.J., 2006. On the interrelations between topography, soil depth, soil moisture, transpiration rates and species distribution at the hillslope scale. Advances in Water Resources, Experimental Hydrology: A Bright Future 29, 293–310. https://doi.org/10.1016/j.advwatres.2005.02.016

V

Vachaud, G., Passerat De Silans, A., Balabanis, P., Vauclin, M., 1985. Temporal Stability of Spatially Measured Soil Water Probability Density Function. Soil Science Society of America Journal 49, 822–828. https://doi.org/10.2136/sssaj1985.03615995004900040006x

Vanderlinden, K., Vereecken, H., Hardelauf, H., Herbst, M., Martínez, G., Cosh, M.H., Pachepsky, Y.A., 2012. Temporal Stability of Soil Water Contents: A Review of Data and Analyses. Vadose Zone Journal 11. https://doi.org/10.2136/vzj2011.0178

Vereecken, H., Huisman, J.A., Bogena, H., Vanderborght, J., Vrugt, J.A., Hopmans, J.W., 2008. On the value of soil moisture measurements in vadose zone hydrology: A review. Water Resour. Res. 44, W00D06. https://doi.org/10.1029/2008WR006829

Vereecken, H., Huisman, J.A., Pachepsky, Y., Montzka, C., van der Kruk, J., Bogena, H., Weihermüller, L., Herbst, M., Martinez, G., Vanderborght, J., 2014. On the spatio-temporal dynamics of soil moisture at the field scale. Journal of Hydrology, Determination of soil moisture: Measurements and theoretical approaches 516, 76–96. https://doi.org/10.1016/j.jhydrol.2013.11.061

W

Wei, W., Feng, X., Yang, L., Chen, L., Feng, T., Chen, D., 2019. The effects of terracing and vegetation on soil moisture retention in a dry hilly catchment in China. Science of The Total Environment 647, 1323–1332. https://doi.org/10.1016/j.scitotenv.2018.08.037

Western, A.W., Grayson, R.B., Blöschl, G., Willgoose, G.R., McMahon, T.A., 1999. Observed spatial organization of soil moisture and its relation to terrain indices. Water Resour. Res. 35, 797–810. https://doi.org/10.1029/1998WR900065

Western, A.W., Zhou, S.-L., Grayson, R.B., McMahon, T.A., Blöschl, G., Wilson, D.J., 2004. Spatial correlation of soil moisture in small catchments and its relationship to dominant spatial hydrological processes. Journal of Hydrology 286, 113–134. https://doi.org/10.1016/j.jhydrol.2003.09.014

Wigmosta, M.S., Nijssen, B., Storck, P., 1994. The Distributed Hydrology Soil Vegetation Model. University of Washington. Chapter 2.

Z

Zhou, Q.Y., Shimada, J., Sato, A., 2001. Three-dimensional spatial and temporal monitoring of soil water content using electrical resistivity tomography. Water Resour. Res. 37, 273–285. https://doi.org/10.1029/2000WR900284

Zhu, X., He, Z., Du, J., Chen, L., Lin, P., & Tian, Q. (2020). Soil moisture temporal stability and spatio-temporal variability about a typical subalpine ecosystem in northwestern China. Hydrological Processes. https://doi.org/10.1002/hyp.13737

Zhuo, L., Dai, Q., Zhao, B., Han, D., 2020. Soil moisture sensor network design for hydrological applications. Hydrology and Earth System Sciences 24, 2577–2591. https://doi.org/10.5194/hess-24-2577-2020

Zreda, M., Desilets, D., Ferré, T.P.A., Scott, R.L., 2008. Measuring soil moisture content non-invasively at intermediate spatial scale using cosmic-ray neutrons. Geophys. Res. Lett. 35, L21402. https://doi.org/10.1029/2008GL035655

Zuecco, G., Penna, D., Borga, M., 2018. Runoff generation in mountain catchments: long-term hydrological monitoring in the Rio Vauz Catchment, Italy. Cuadernos de investigación geográfica / Geographical Research Letters 397–428.

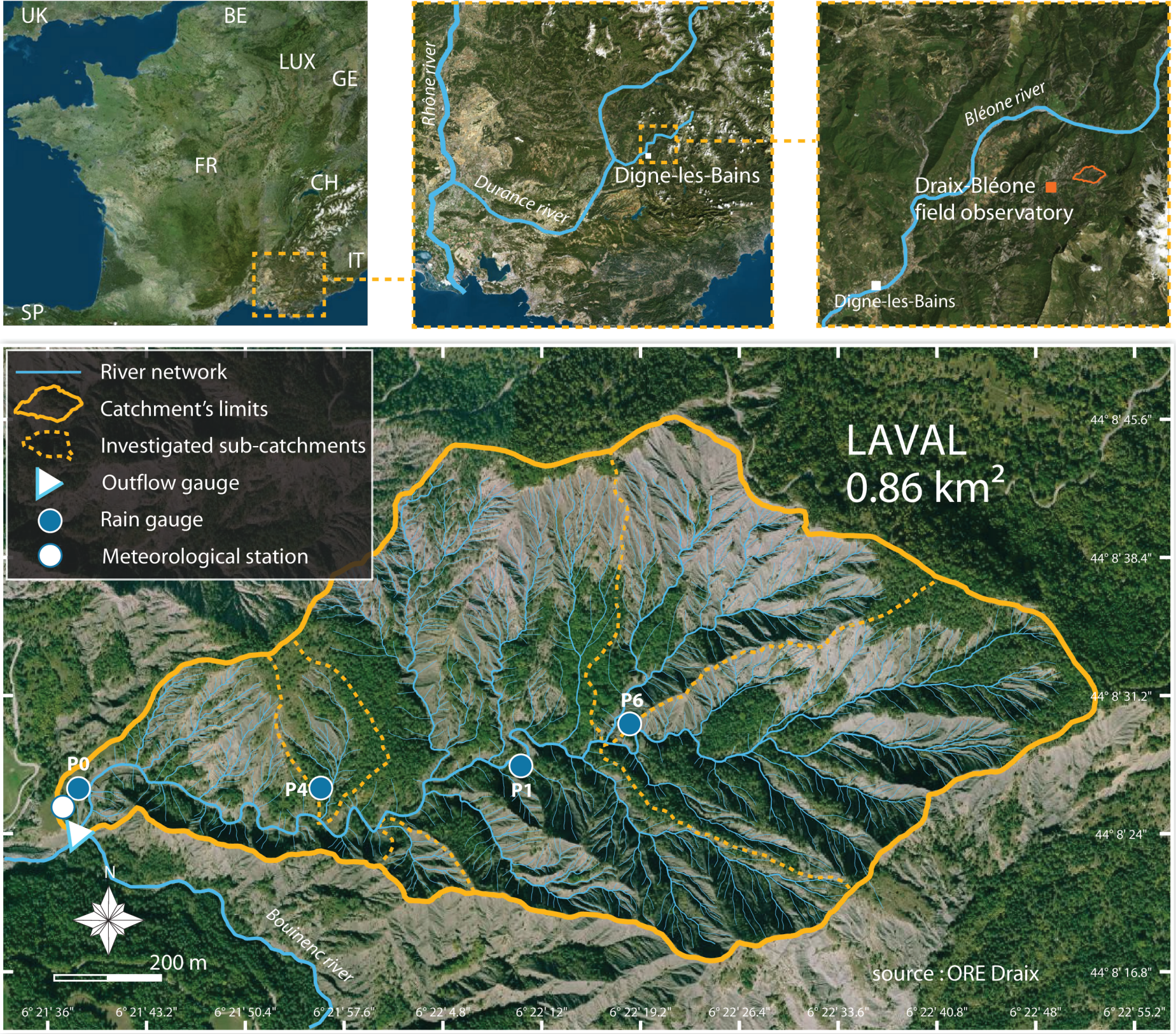
UK
BE
LUX
GE
FR
CH
IT
SP
Rhône river
Durance river
Digne-les-Bains
Bléone river
Draix-Bléone
field observatory
Digne-les-Bains
River network
Catchment's limits
Investigated sub-catchments
Outflow gauge
Rain gauge
Meteorological station
LAVAL
0.86 km²
P0
P4
P1
P6
N
200 m
Bouinenc river
source : ORE Draix
44° 8' 45.6"
44° 8' 38.4"
44° 8' 31.2"
44° 8' 24"
44° 8' 16.8"
6° 21' 36"
6° 21' 43.2"
6° 21' 50.4"
6° 21' 57.6"
6° 22' 4.8"
6° 22' 12"
6° 22' 19.2"
6° 22' 26.4"
6° 22' 33.6"
6° 22' 40.8"
6° 22' 48"
6° 22' 55.2"

1/ Capacitance sensors nework design, setup and calibration

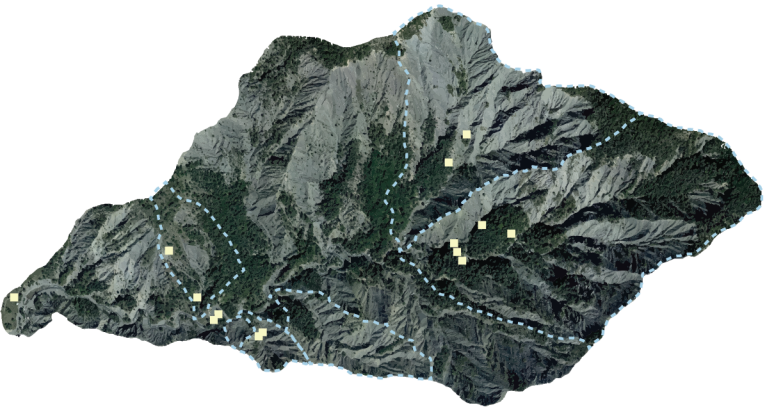

2/ SWC, rainfall and outflow monitoring

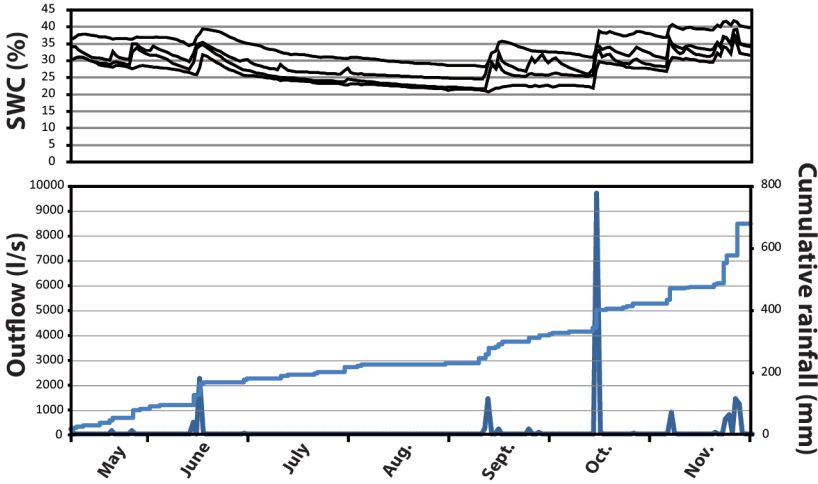

3/ SWC estimation using spatial interpolation based on geographical variables

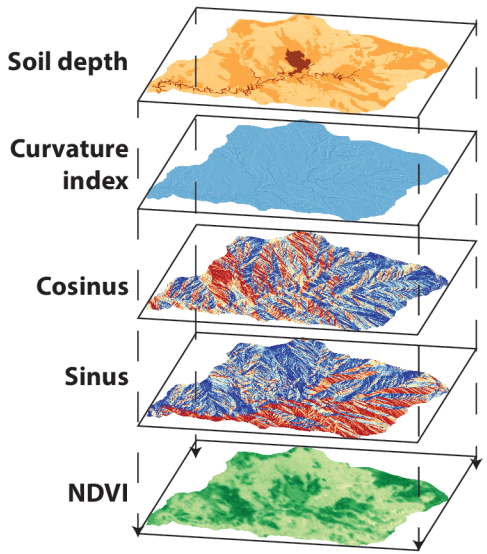

4/ Identifying the dominant flow mechanism from the wetting curve maximum slope method

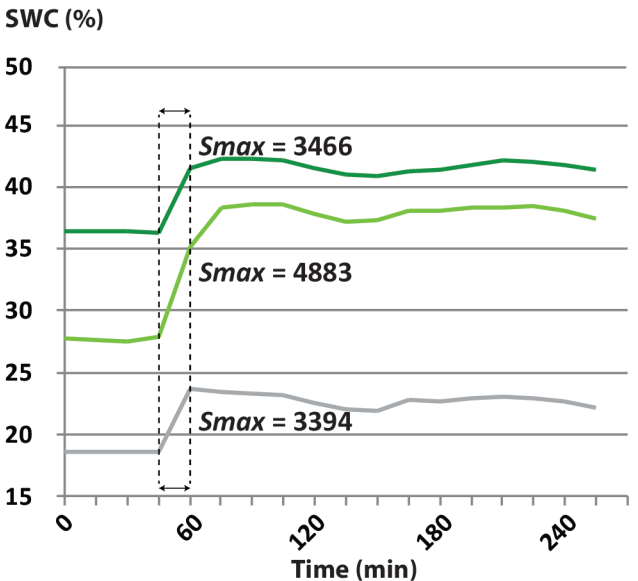

1/ Sub-catchments classification

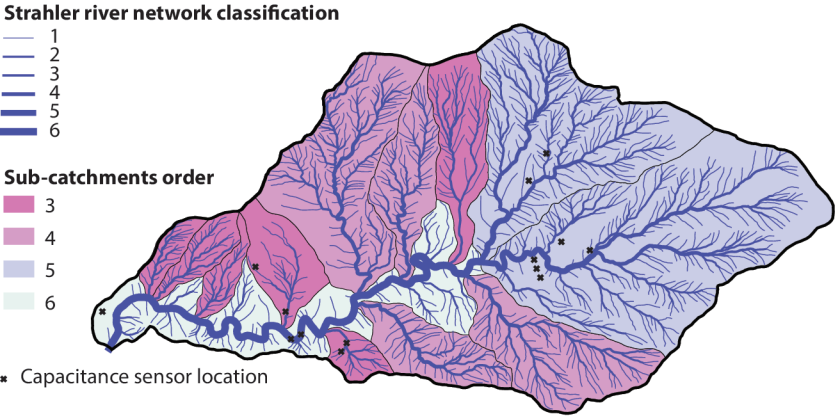

2/ Identification of theoretical surface flow concentration areas

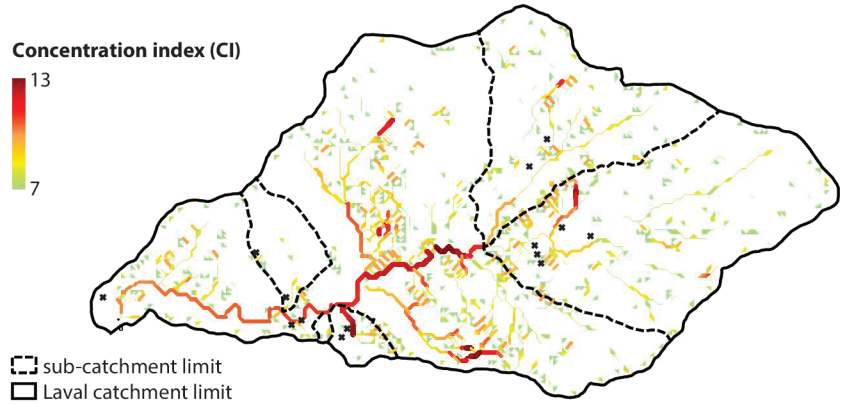

3/ Selection of 4 sub-catchments based on land uses

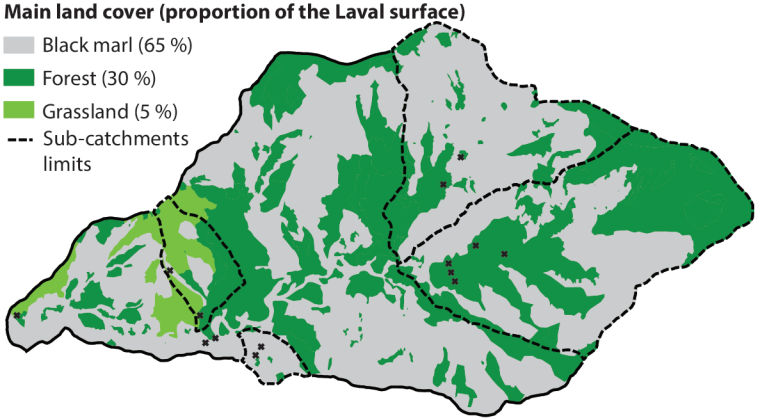

4/ Soil-vegetation map

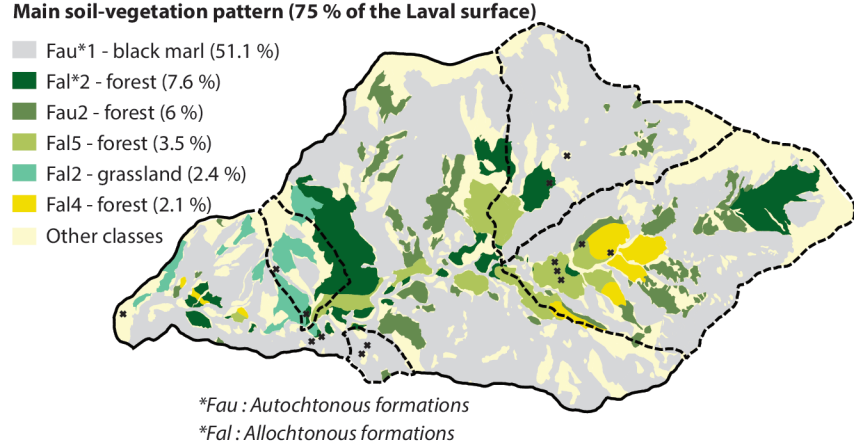

Fau : Autochtonous formations
Fal : Allochtonous formations

5/ SWC monitoring network

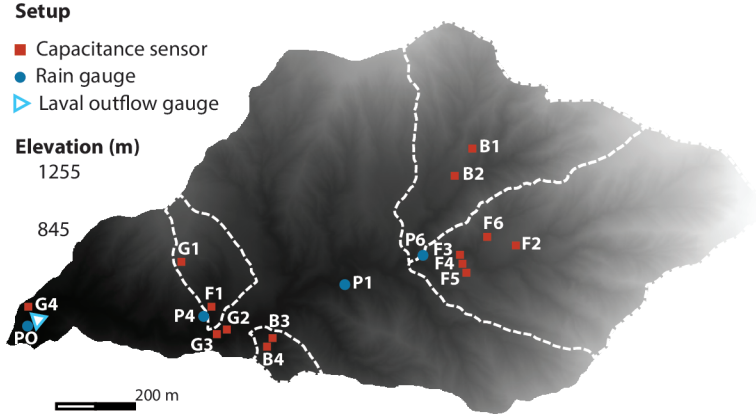

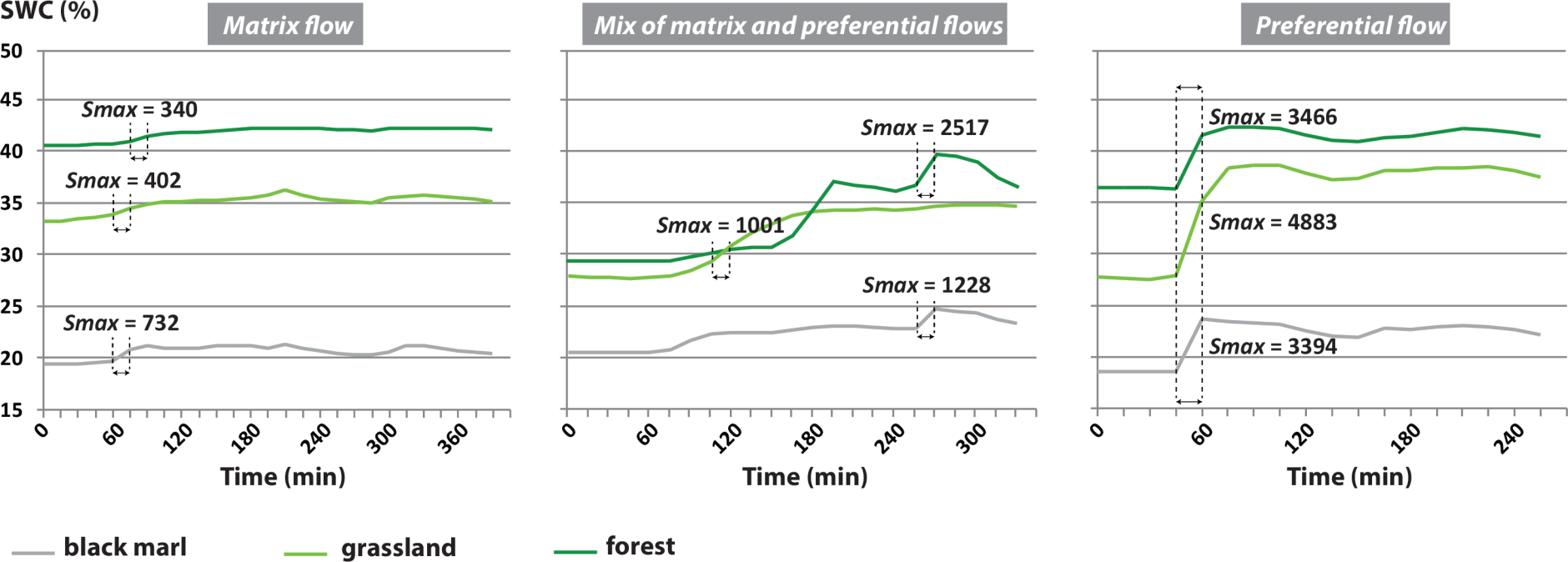
SWC (%)
Matrix flow
Mix of matrix and preferential flows
Preferential flow
Smax = 340
Smax = 402
Smax = 732
Smax = 2517
Smax = 1001
Smax = 1228
Smax = 3466
Smax = 4883
Smax = 3394
Time (min)
black marl
grassland
forest

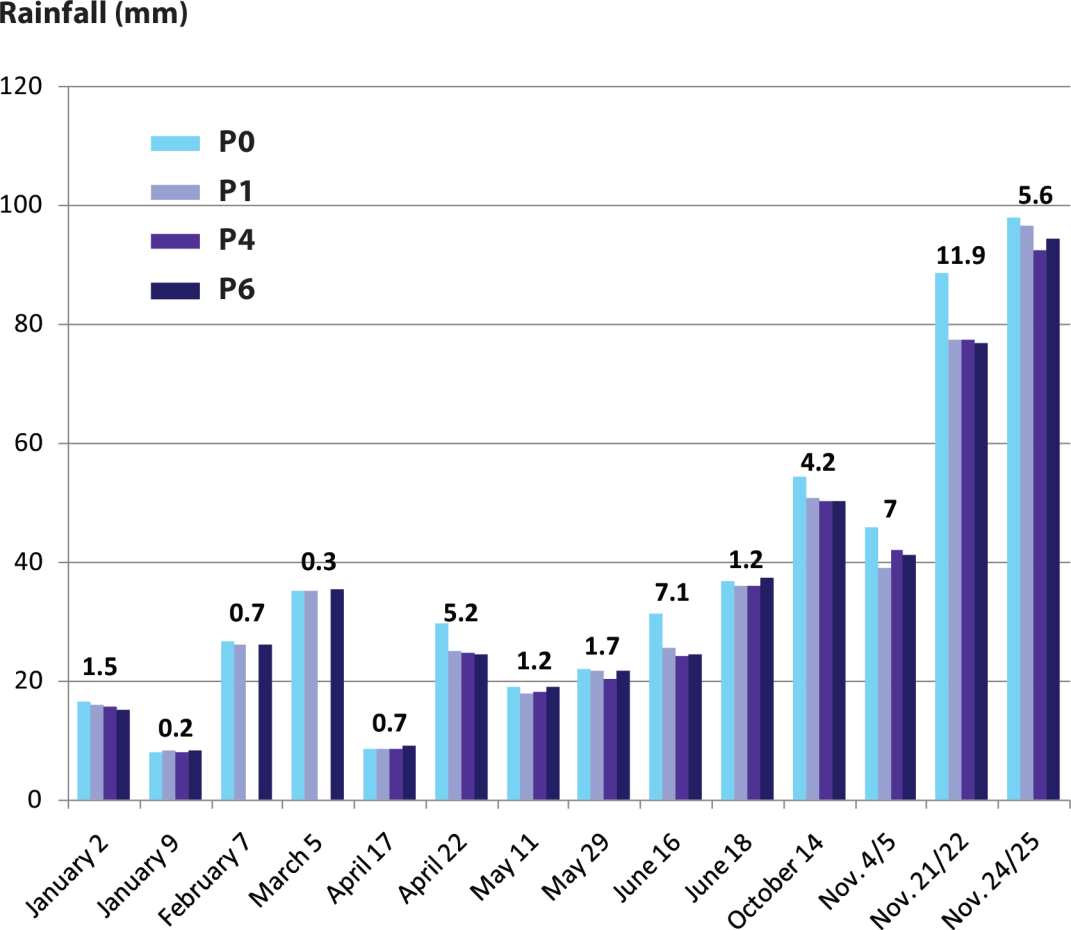
Rainfall (mm)
120
100
80
60
40
20
0
P0
P1
P4
P6
1.5
0.2
0.7
0.3
0.7
5.2
1.2
1.7
7.1
1.2
4.2
7
11.9
5.6
January 2
January 9
February 7
March 5
April 17
April 22
May 11
May 29
June 16
June 18
October 14
Nov. 4/5
Nov. 21/22
Nov. 24/25

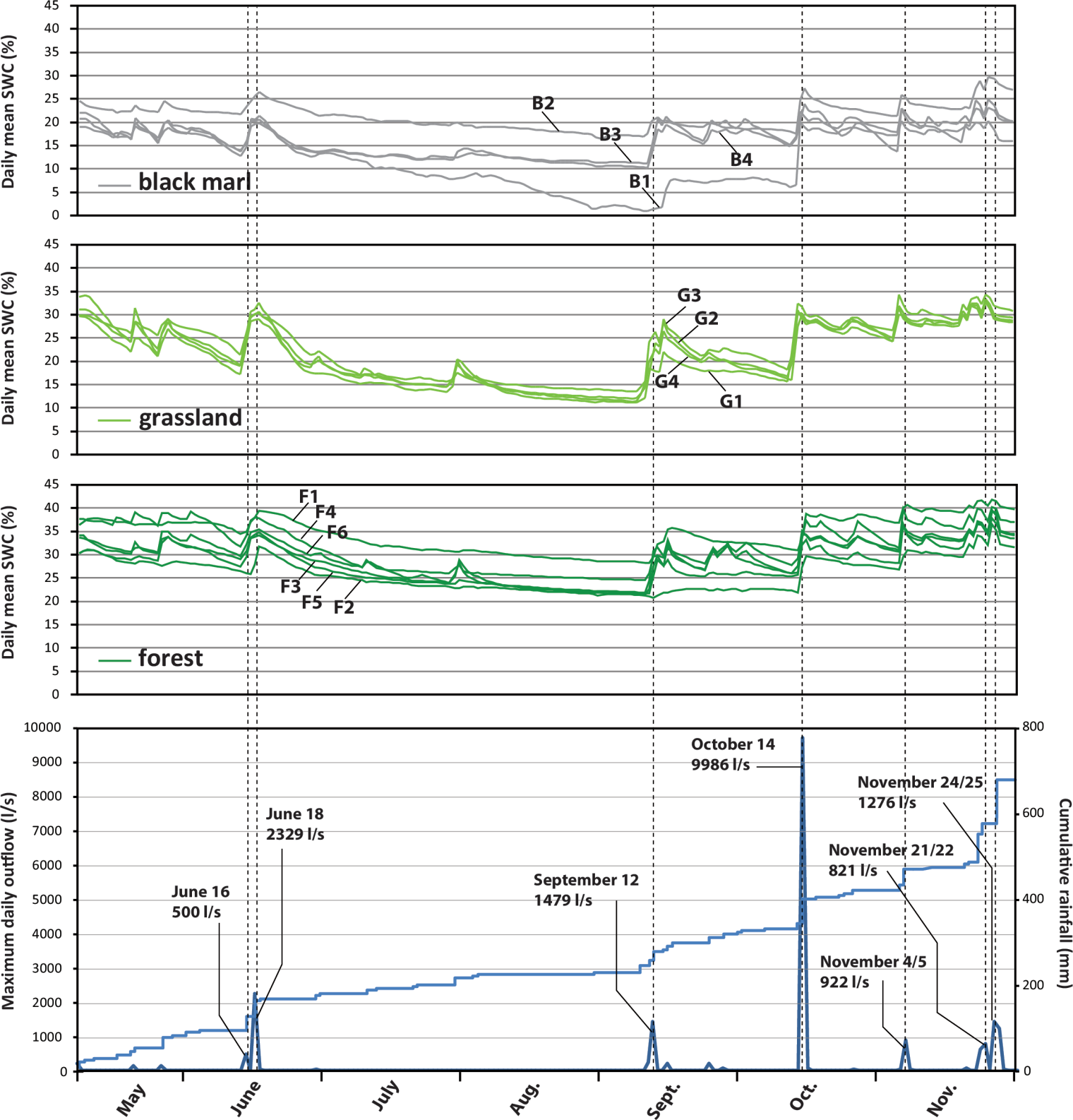
Daily mean SWC (%)
black marl
B2
B3
B1
B4
grassland
G3
G2
G4
G1
forest
F1
F4
F6
F3
F5
F2
Maximum daily outflow (l/s)
Cumulative rainfall (mm)
June 16
500 l/s
June 18
2329 l/s
September 12
1479 l/s
October 14
9986 l/s
November 21/22
821 l/s
November 24/25
1276 l/s
November 4/5
922 l/s
May
June
July
Aug.
Sept.
Oct.
Nov.

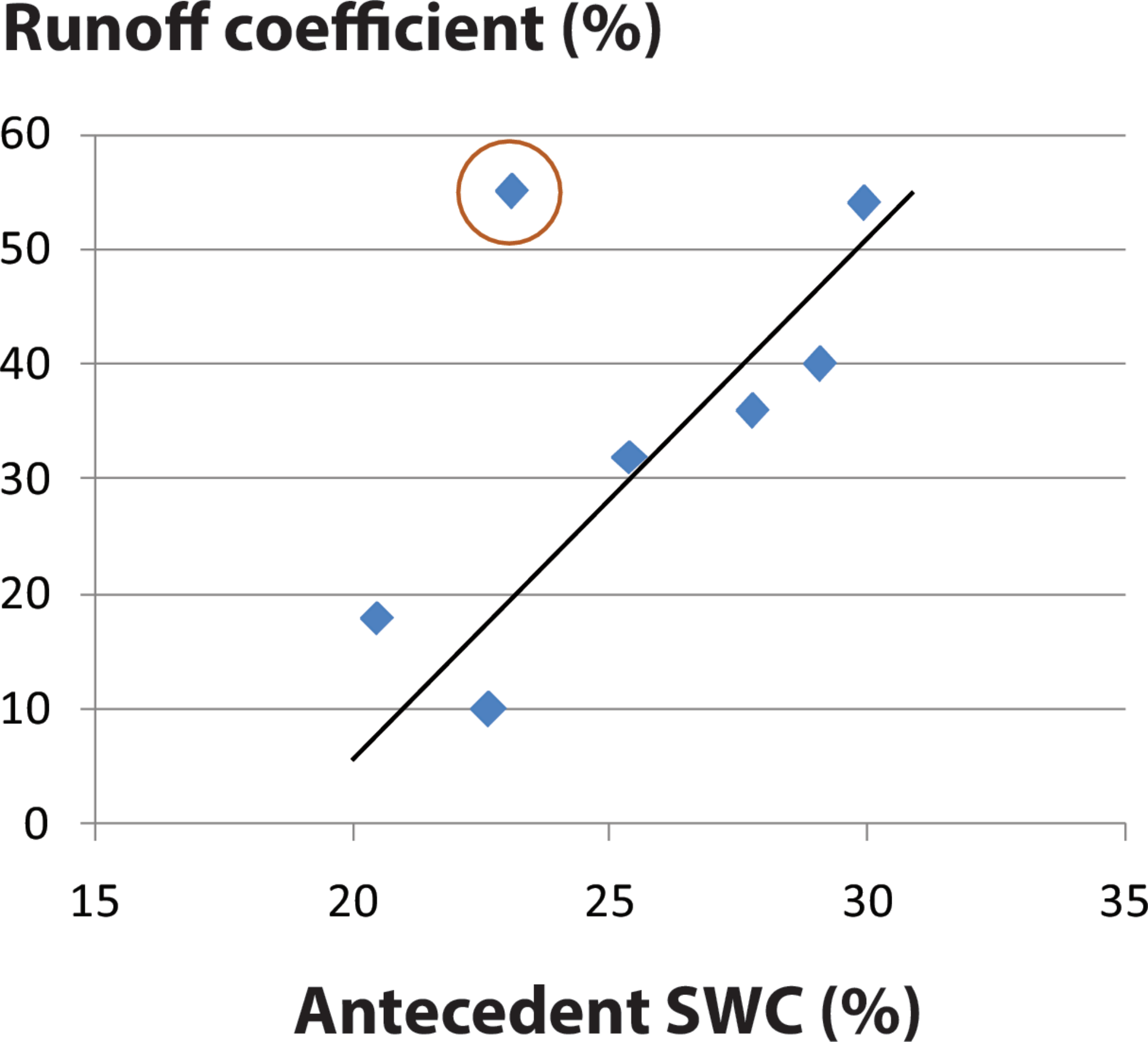
Runoff coefficient (%)
60
50
40
30
20
10
0
15
20
25
30
35
Antecedent SWC (%)

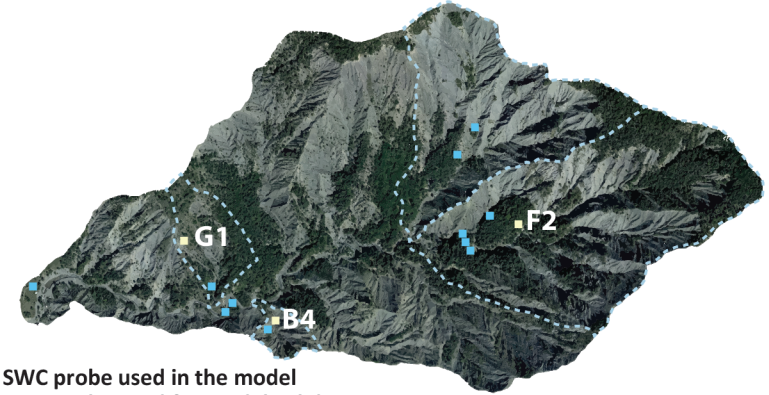

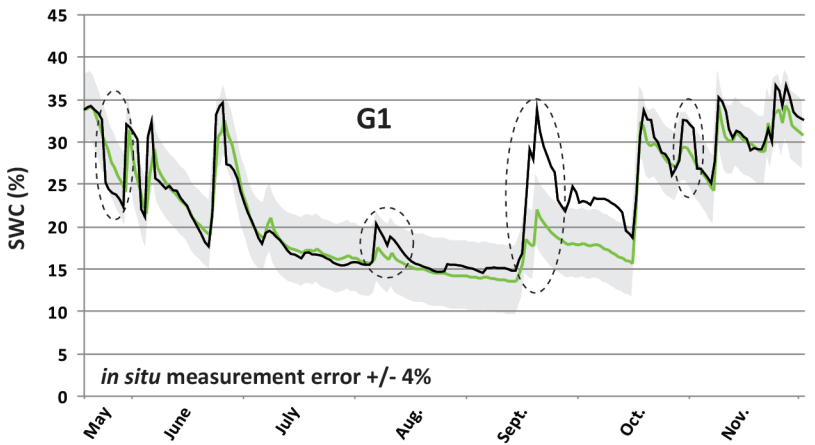

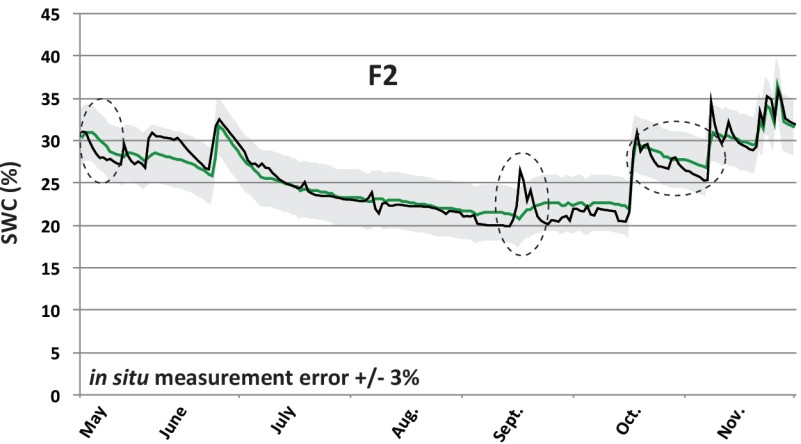

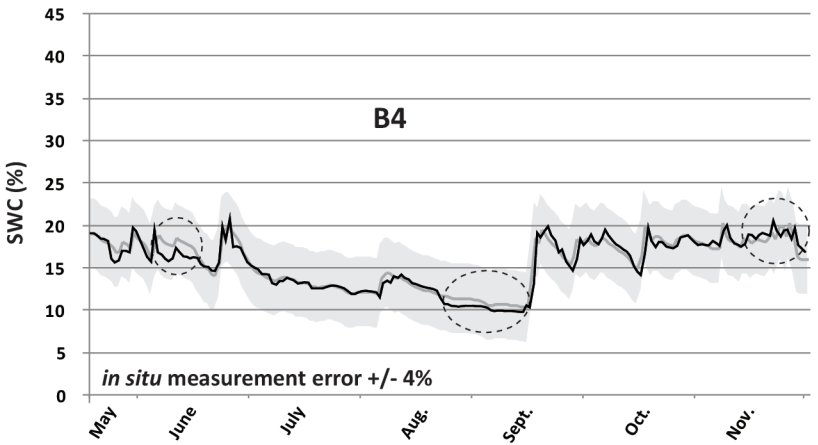

SWC measured in black marl

SWC measured in grassland

SWC measured in forest

Estimated SWC

In situ measurement error

Main overestimations and underestimations

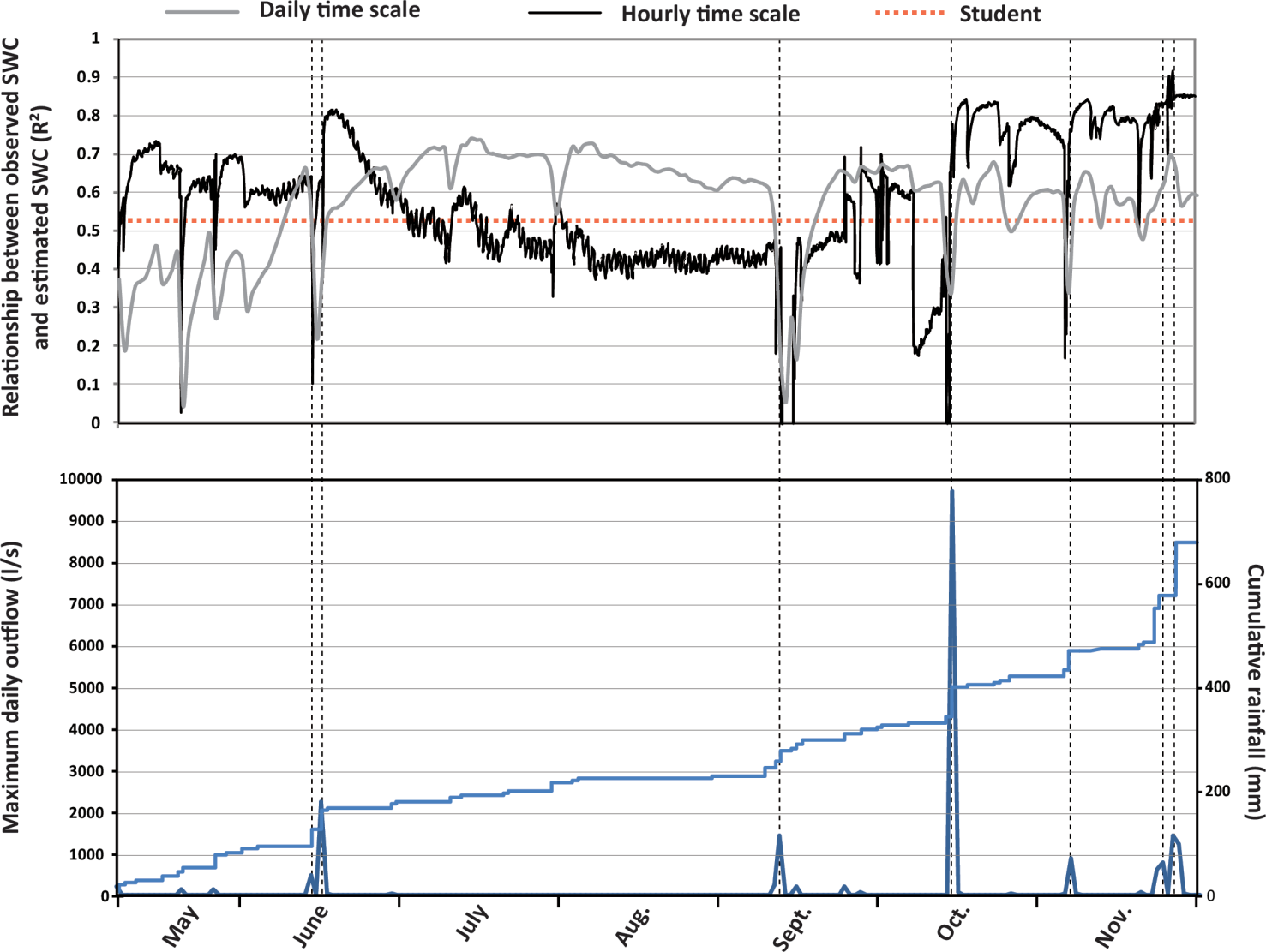
Daily time scale
Hourly time scale
Student
Relationship between observed SWC and estimated SWC (R²)
1
0.9
0.8
0.7
0.6
0.5
0.4
0.3
0.2
0.1
0
Maximum daily outflow (l/s)
10000
9000
8000
7000
6000
5000
4000
3000
2000
1000
0
800
600
400
200
0
Cumulative rainfall (mm)
May
June
July
Aug.
Sept.
Oct.
Nov.

Relationship between measured and estimated SWC (R^2)

	B1	B2	B3	B4	G1	G2	G3	G4	F1	F2	F3	F4	F5	F6
Daily time scale	0.394	0.533	0.932	0.889	0.189	0.996	0.995	0.692	0.607	0.802	0.886	0.952	0.861	0.528
Hourly time scale	0.393	0.515	0.933	0.884	0.167	0.996	0.995	0.691	0.605	0.782	0.881	0.949	0.859	0.529

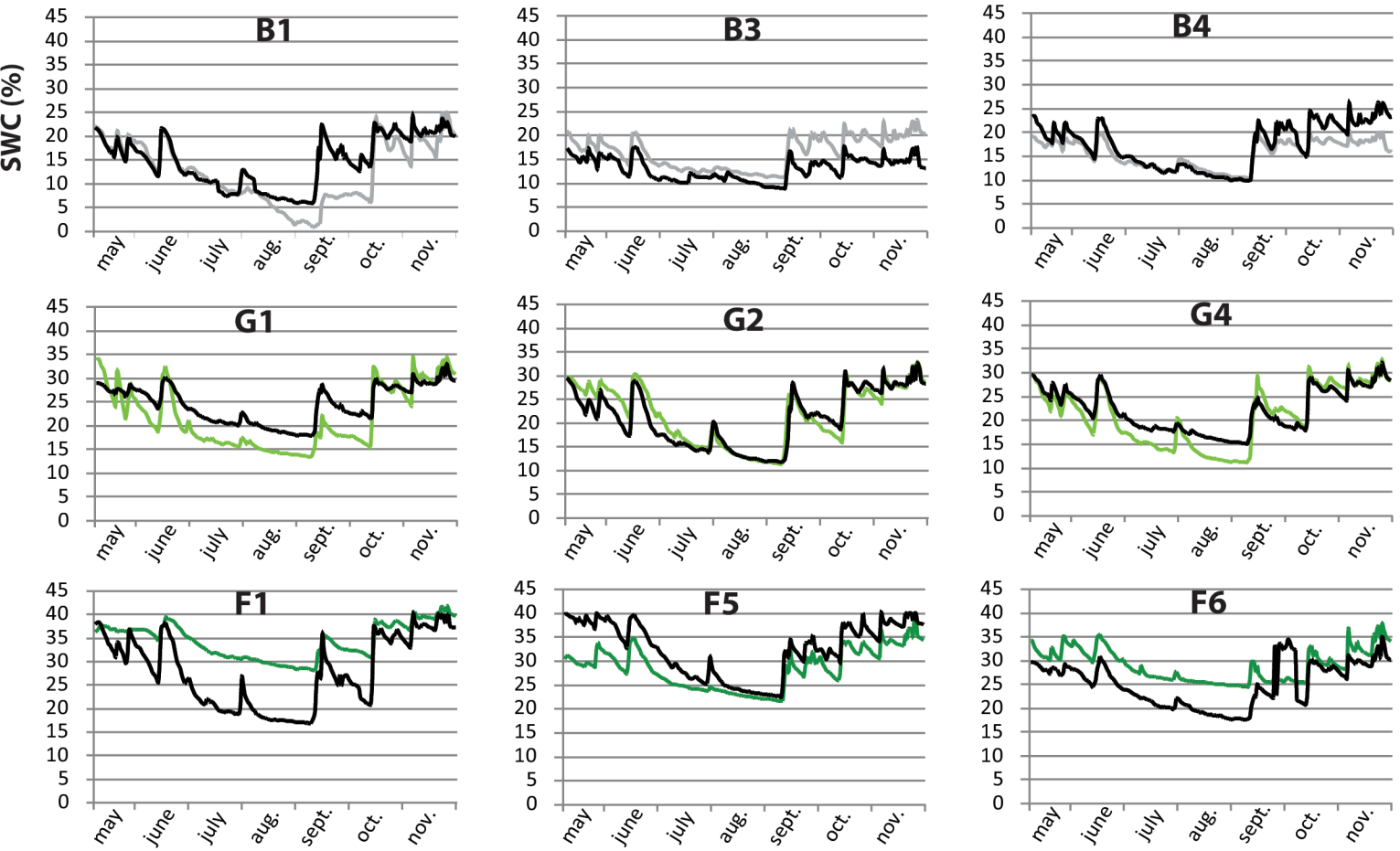

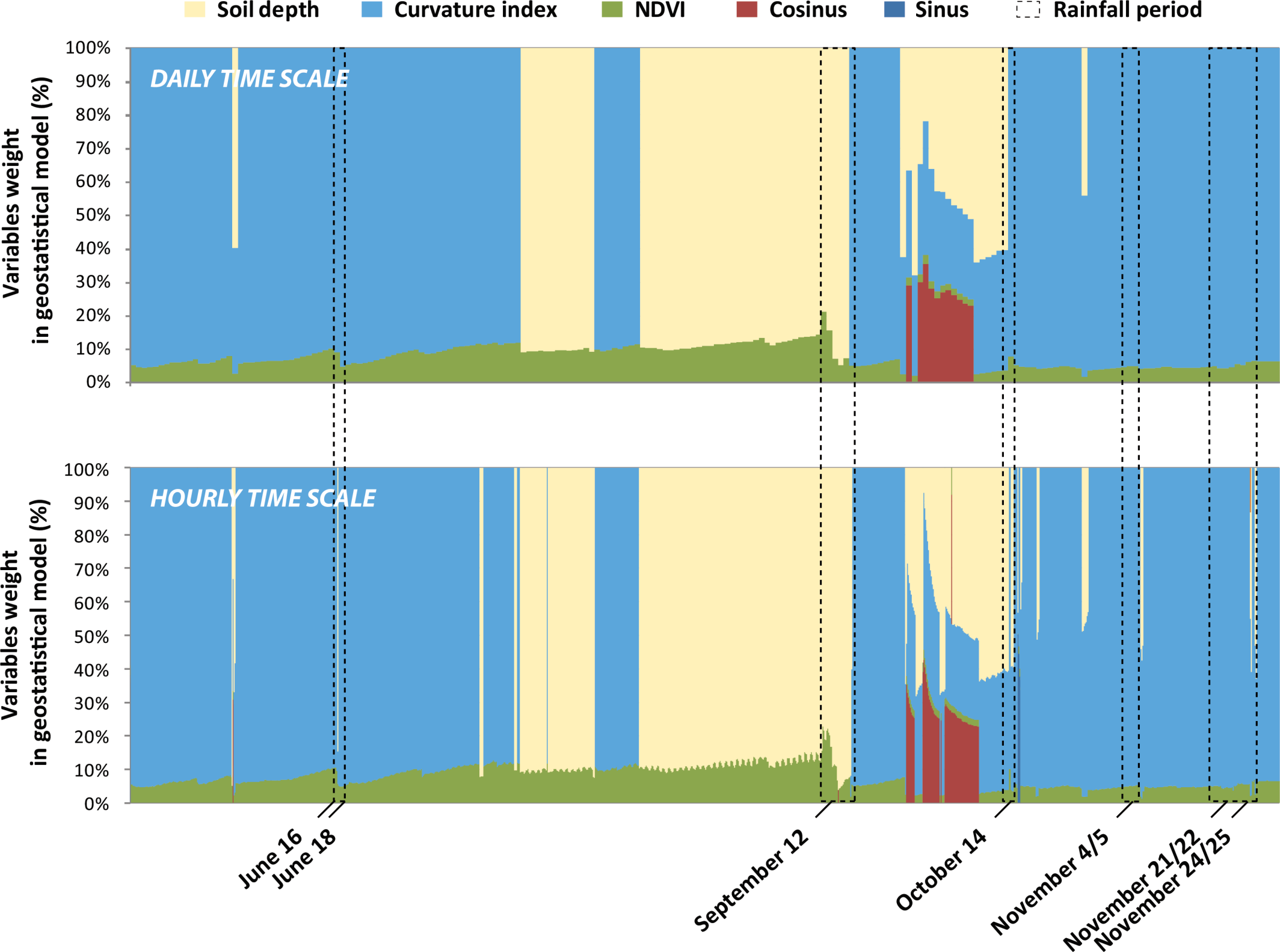
Soil depth
Curvature index
NDVI
Cosinus
Sinus
Rainfall period
DAILY TIME SCALE
HOURLY TIME SCALE
Variables weight in geostatistical model (%)
100%
90%
80%
70%
60%
50%
40%
30%
20%
10%
0%
June 16
June 18
September 12
October 14
November 4/5
November 21/22
November 24/25

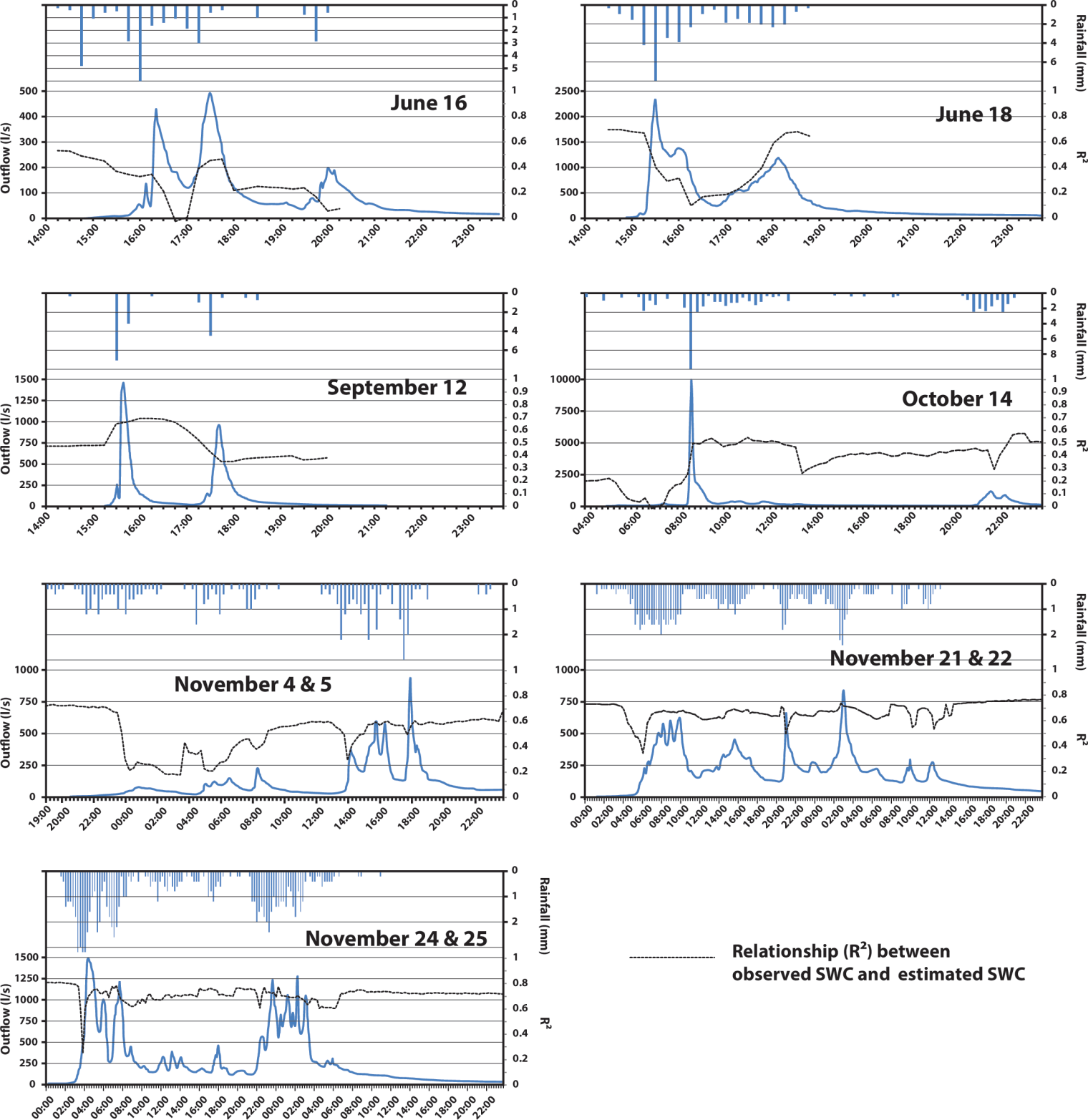
June 16
June 18
September 12
October 14
November 4 & 5
November 21 & 22
November 24 & 25
Outflow (l/s)
Rainfall (mm)
R²
Relationship (R²) between observed SWC and estimated SWC

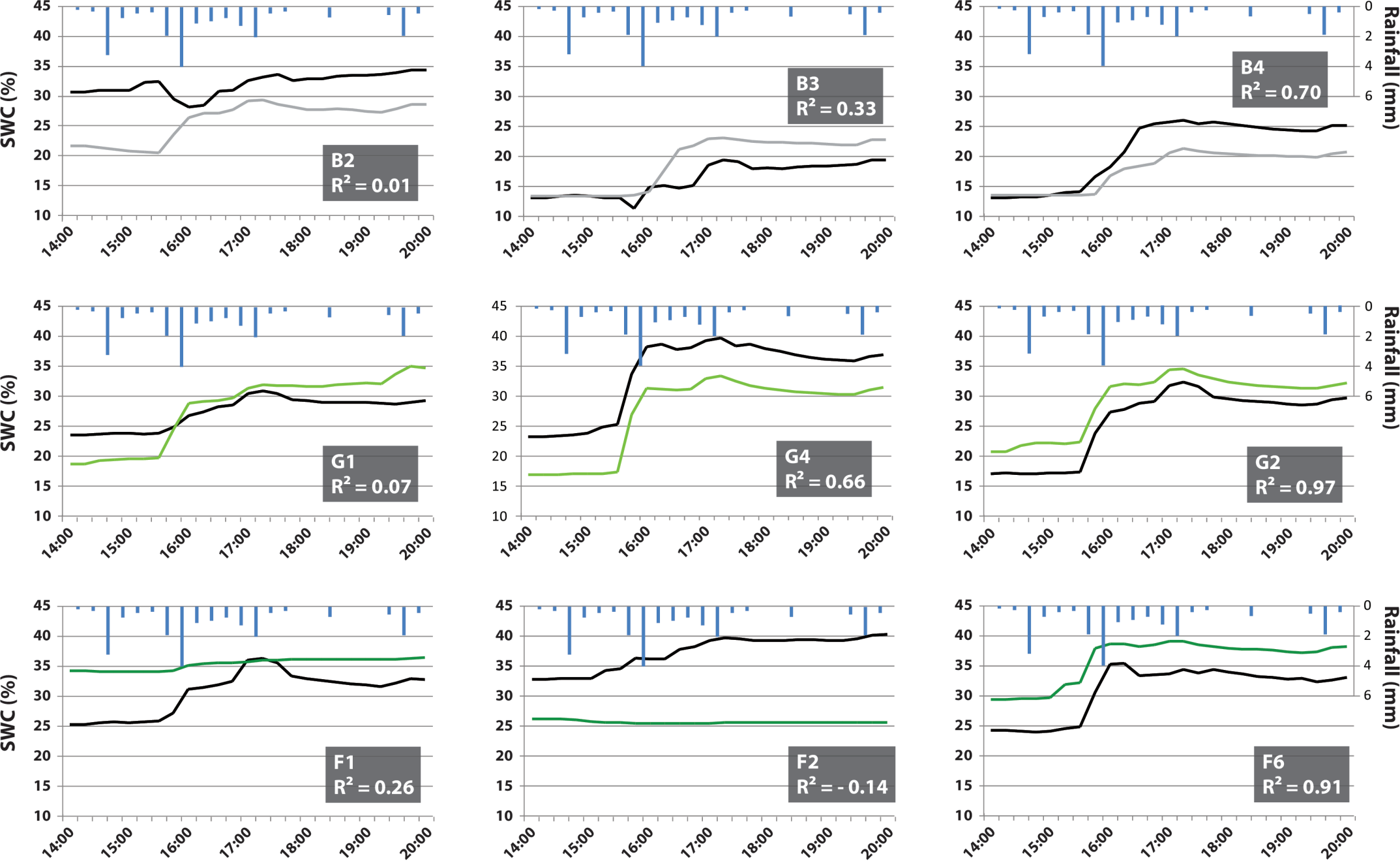
SWC (%)
Rainfall (mm)
B2
R² = 0.01
B3
R² = 0.33
B4
R² = 0.70
G1
R² = 0.07
G4
R² = 0.66
G2
R² = 0.97
F1
R² = 0.26
F2
R² = - 0.14
F6
R² = 0.91
14:00
15:00
16:00
17:00
18:00
19:00
20:00
SWC measured in black marl
SWC measured in grassland
SWC measured in forest
estimated SWC

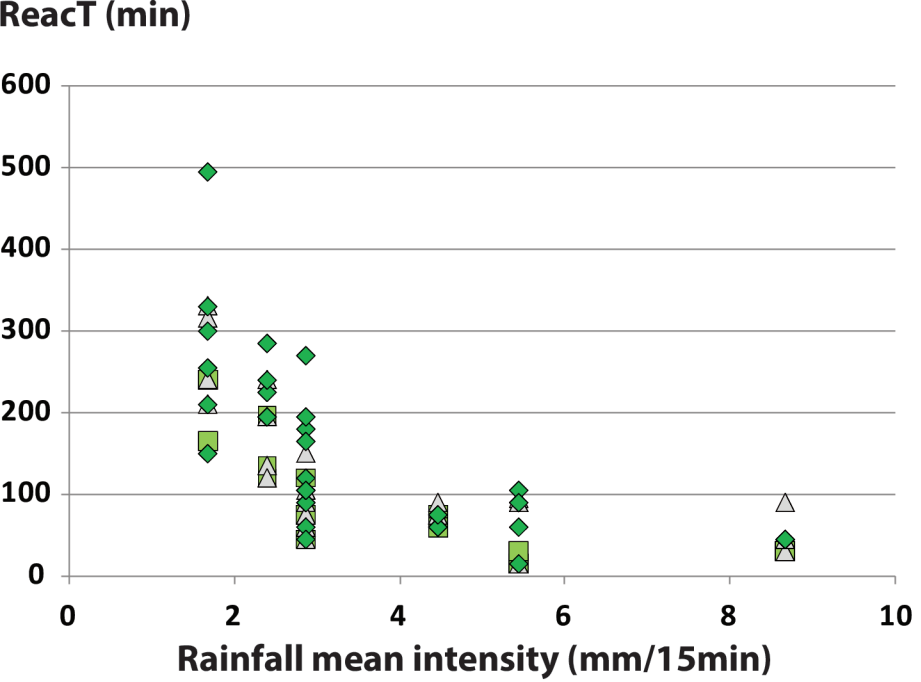
ReacT (min)
600
500
400
300
200
100
0
0
2
4
6
8
10
Rainfall mean intensity (mm/15min)

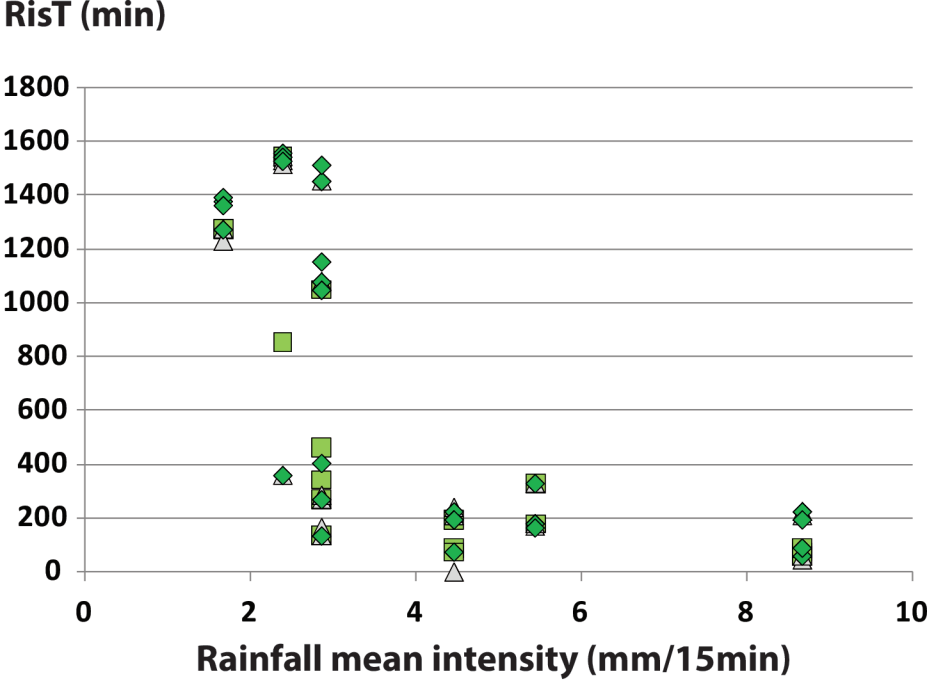
RisT (min)
1800
1600
1400
1200
1000
800
600
400
200
0
0
2
4
6
8
10
Rainfall mean intensity (mm/15min)

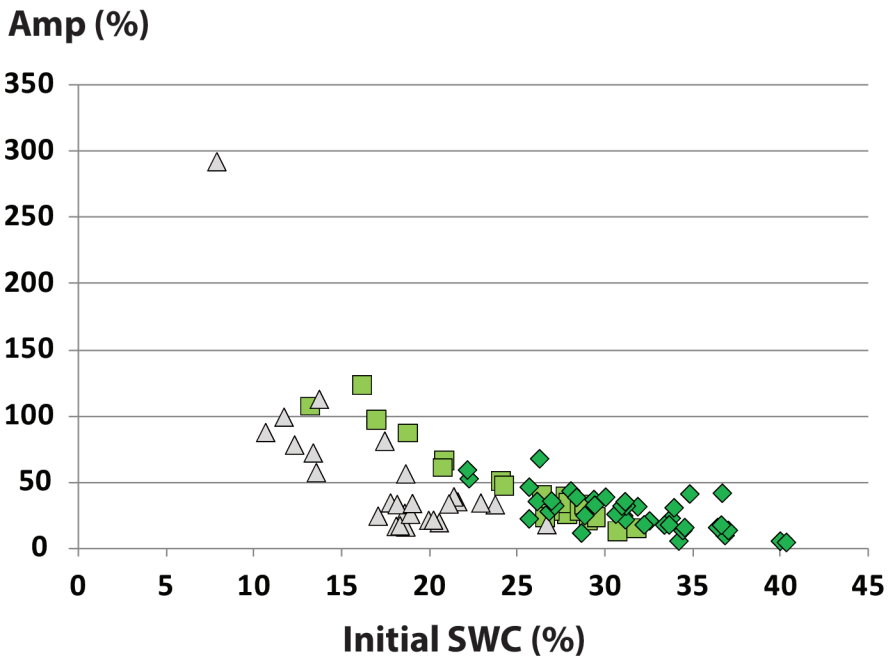
Amp (%)
350
300
250
200
150
100
50
0
0
5
10
15
20
25
30
35
40
45
Initial SWC (%)


SWC monitored land cover
Black Marl
Forest
Grassland

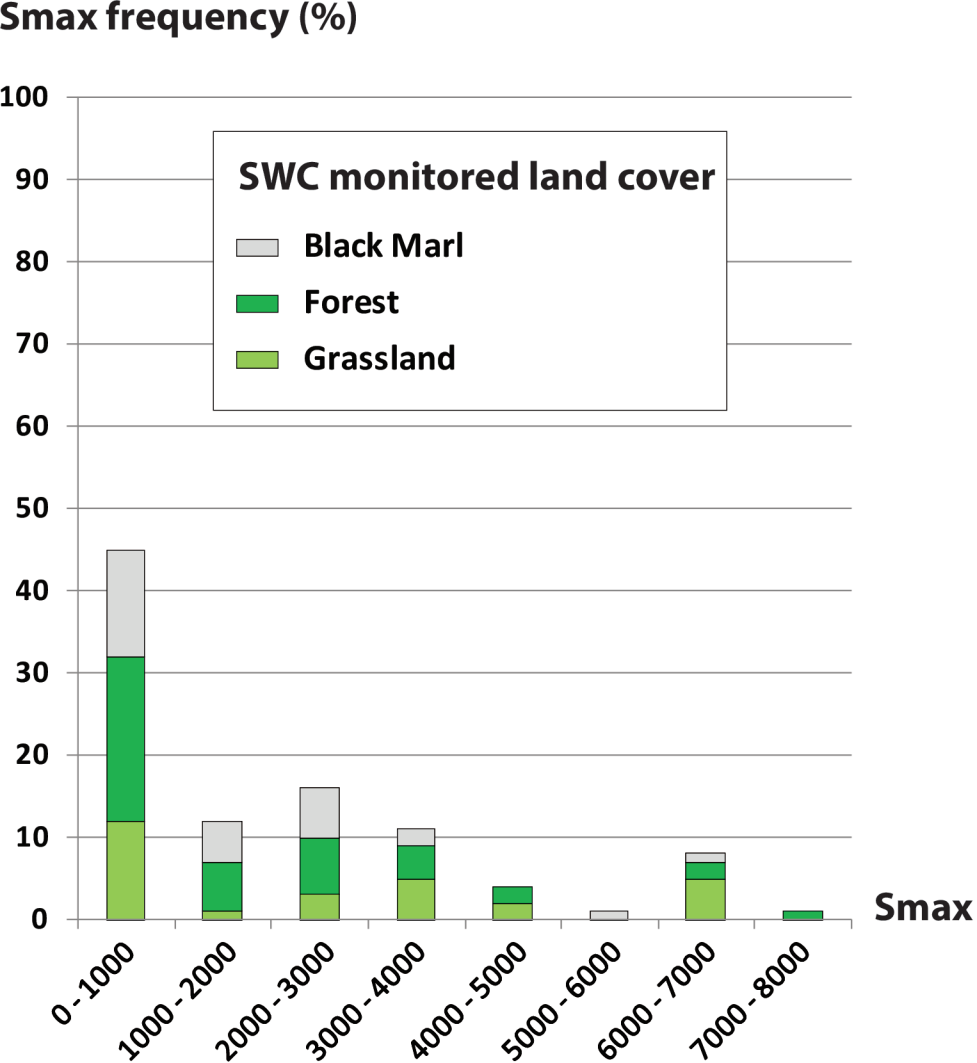
Smax frequency (%)
100
90
80
70
60
50
40
30
20
10
0
SWC monitored land cover
Black Marl
Forest
Grassland
Smax
0 - 1000
1000 - 2000
2000 - 3000
3000 - 4000
4000 - 5000
5000 - 6000
6000 - 7000
7000 - 8000

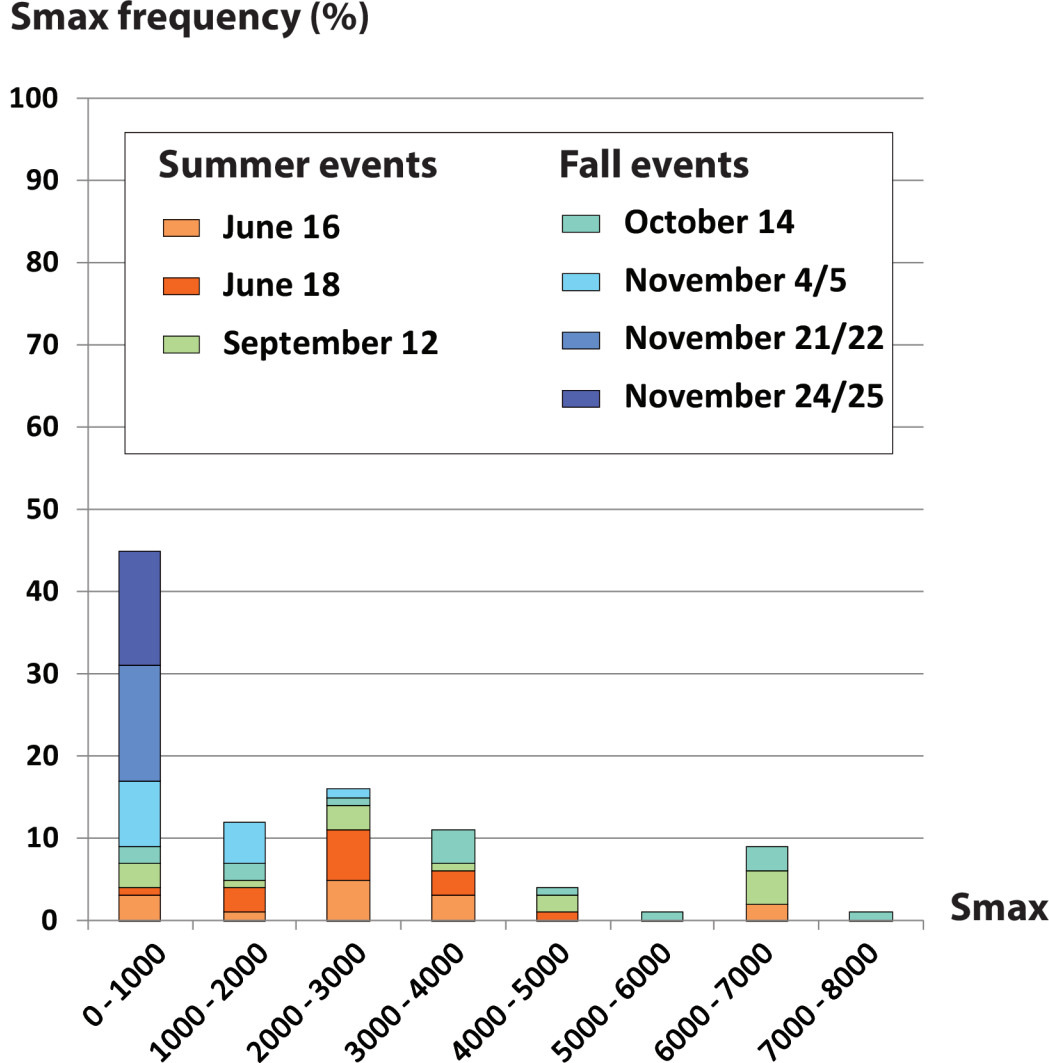
Smax frequency (%)
100
90
80
70
60
50
40
30
20
10
0
Summer events
June 16
June 18
September 12
Fall events
October 14
November 4/5
November 21/22
November 24/25
Smax
0 - 1000
1000 - 2000
2000 - 3000
3000 - 4000
4000 - 5000
5000 - 6000
6000 - 7000
7000 - 8000

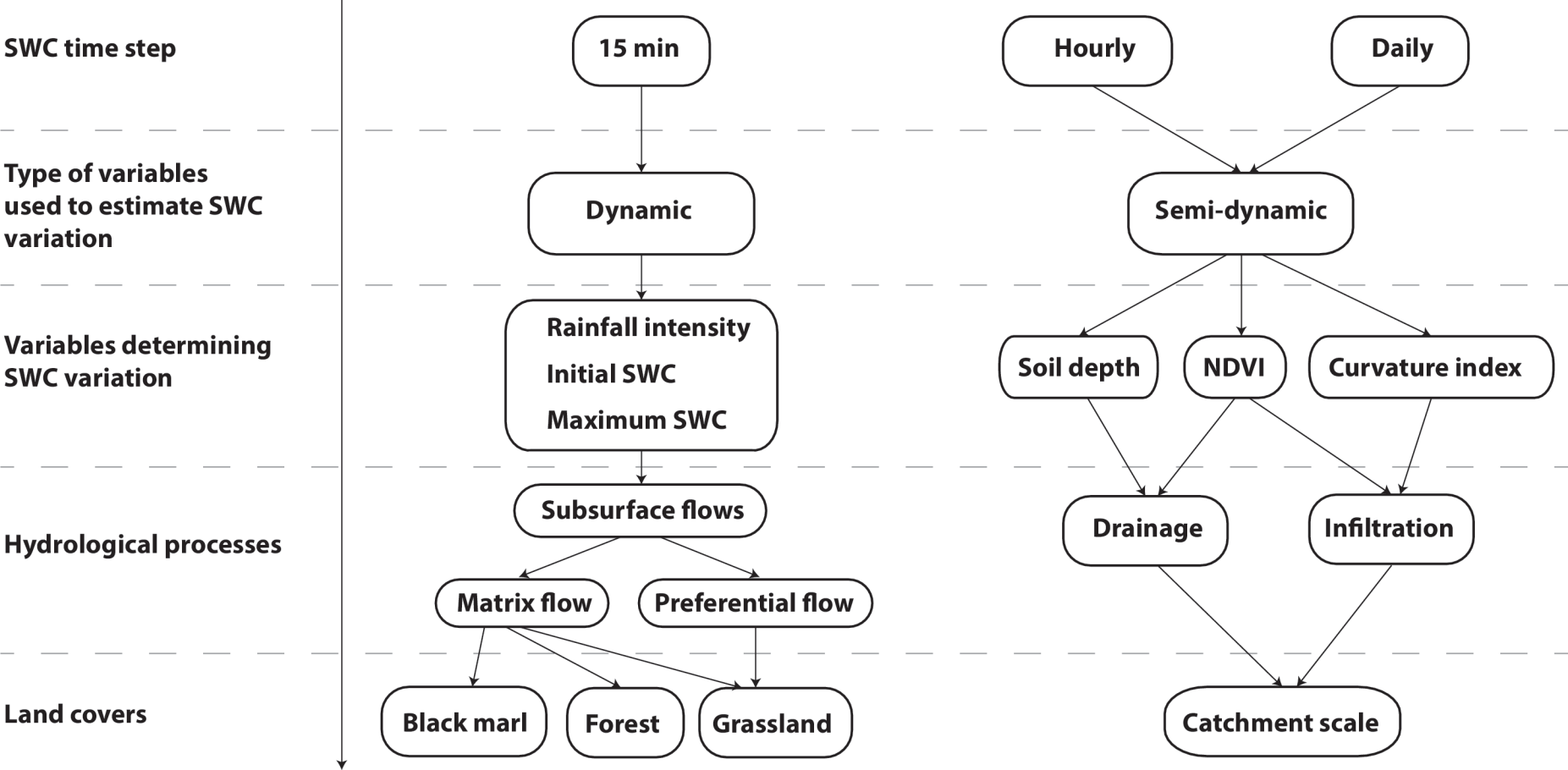
SWC time step
Type of variables used to estimate SWC variation
Variables determining SWC variation
Hydrological processes
Land covers
15 min
Hourly
Daily
Dynamic
Semi-dynamic
Rainfall intensity
Initial SWC
Maximum SWC
Soil depth
NDVI
Curvature index
Subsurface flows
Drainage
Infiltration
Matrix flow
Preferential flow
Black marl
Forest
Grassland
Catchment scale